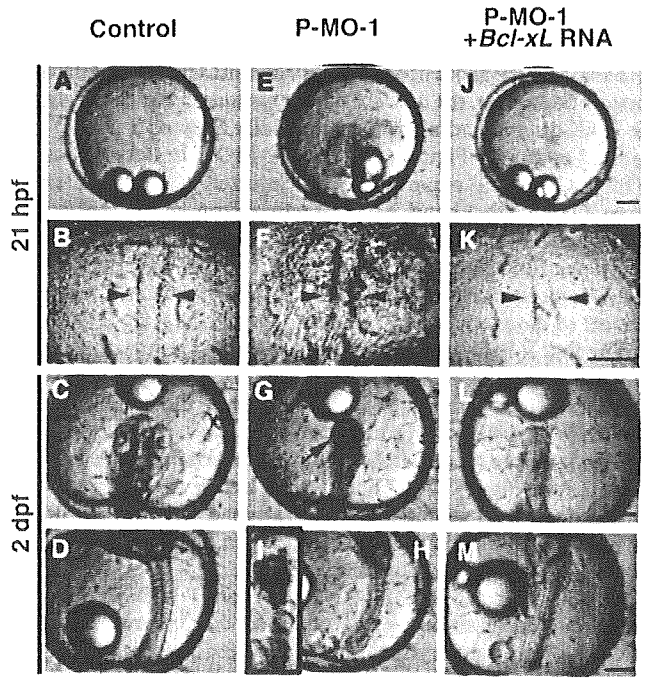

Fig. 5. Effects of GlcAT-P-depletion on medaka development. Morphological analysis of GlcAT-P-depleted medaka embryos. Control (**A–D**), P-MO-1-injected and *Bcl-xL* RNA and P-MO-1 co-injected embryos observed at 21 hpf (the 75% epiboly stage) (**A, B, E, F, J,** and **K**) and 2 dpf (**C, D, G, H, I, L,** and **M**). Panels **B, F,** and **K** are magnified views of the embryos shown in **A, E,** and **J**, respectively. Arrowheads indicate the edges of the embryonic body (**B, F,** and **K**). In panels **G** and **H**, the embryo in mildly affected group is shown, whereas panel **I** represents the embryo in severely affected group (see the text for detail). An arrow in panel **G** indicates eyes, which are no longer recognizable in a severely affected embryo shown in **I**. All the panels are in dorsal view, animal/anterior to the top. Bars, 200 μm.

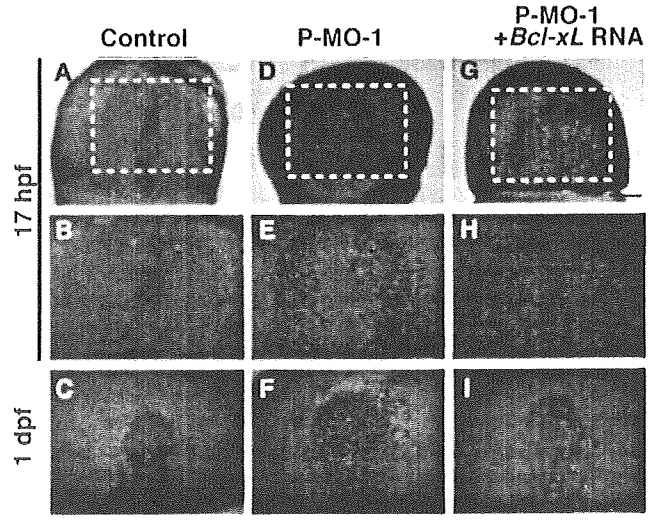

Fig. 6. TUNEL staining of embryos. Control, P-MO-1-injected and *Bcl-xL* RNA and P-MO-1 co-injected embryos at 17 hpf (the 50% epiboly stage) (**A, B, D, E, G,** and **H**) or 1 dpf (**C, F,** and **I**). Dot-like stainings represent apoptotic cells. The number of apoptotic cells was significantly increased by P-MO-1-injected. (**D–F**) Note that apoptosis was efficiently inhibited by *Bcl-xL* mRNA co-injection (compare panels **E** and **H** or **F** and **I**). Panels **B, E,** and **H** are magnified view of regions surrounded in white dashed lines in **A, D,** and **G**, respectively. All the panels are in dorsal view, animal/anterior to the top. Bars, 200 μm.

of P-MO-1-injected embryos), head hypoplasia was observed, although two eyes were still recognizable (an example shown in Figure 5G, an arrow indicates the forming eyes). In these embryos, the organogenesis of the head region seemed to be defective, as the whole head structure was smaller than that in control embryos (compare Figure 5C and G). Somitegenesis did take place in these embryos, although the size and number of somites were reduced and the anterior–posterior length of the embryos seemed to be shorter than that in the control (Figure 5D and H). In the severely affected group (Table I, 42% of P-MO-1-injected embryos), defects in the head organogenesis were much more evident and the eyes were no longer recognized (Figure 5I). Moreover, the trunk region appeared to be degenerated in this group of the embryos, although a sign of somitogenesis was still observed. These results demonstrated that the HNK-1 carbohydrate synthesized by GlcAT-Ps plays essential roles in embryonic organogenesis, especially in the head region. The injection of P-MO-2 essentially gave the same result as P-MO-1 injection, albeit there was higher penetrance even at a lower dose (Table I; abnormal in 65% of the embryos by 5 ng P-MO-1 injection, in contrast to 74% on 1 ng P-MO-2 injection).

We further examined whether the phenotypes induced by the injection of P-MO-1 could be reversed by co-expression of GlcAT-P. We synthesized RNA for *GlcAT-P* that lacks target sequences of the P-MO-1 but still has the ability to synthesize the HNK-1 carbohydrate and co-injected it along with P-MO-1. The injection of the various amount of *GlcAT-P* RNA did not reverse the defect of development (data not shown), allowing us to surmise that the ectopic expression of *GlcAT-P* itself causes severe developmental defects (as shown above).

While analyzing the effect of GlcAT-P depletion on early development, we noticed the appearance of dark-stained cells around the presumptive neuroectoderm during gastrulation and the head region at 1–2 dpf in GlcAT-P-depleted embryos (see Figure 5). As this could be a sign of apoptotic cell death, we carried out two different assays to detect apoptotic cells, TUNEL staining and acridine orange whole mount staining, of the embryos at both stages. As expected, massive ectopic apoptosis was observed in the regions of GlcAT-P-depleted embryos where the dark-stained cells were observed, whereas no significant staining was seen in control embryos with either assay methods (Figure 6A–F and data not shown). These results raised the possibility that the defective head morphogenesis observed in GlcAT-P-depleted embryos is caused by the enhanced apoptosis. We thought GlcAT-P depletion specifically resulted in the apoptosis, however it has been reported that apoptosis in the head region was often caused by off-targeting effects of MO (Robu et al. 2007). To examine this, we investigated whether or not the phenotypic outcome observed in GlcAT-P-depleted embryos was altered when the apoptosis was blocked. For this purpose, we used MO against *p53* for inhibiting apoptosis as previously reported (Robu et al. 2007). Unfortunately, p53 MO we used affected embryonic development by itself at various doses. These results suggested that p53 is more essential for medaka embryonic development than zebrafish. Alternatively,

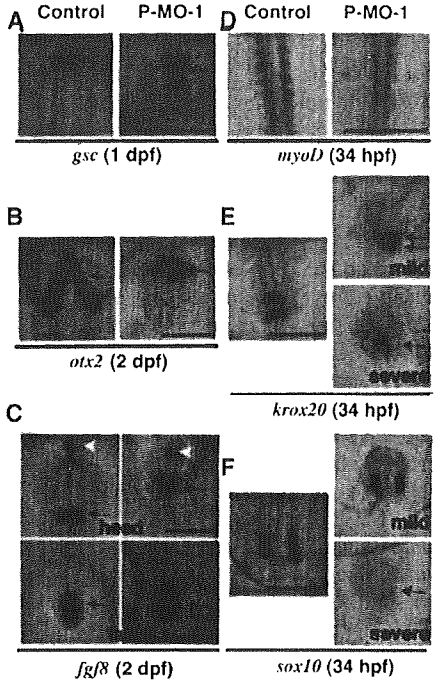

Fig. 7. In situ hybridization analysis of GlcAT-P-depleted embryos. (**A**) *Gsc* expression at 1 dpf. Red arrow in each panel indicates the prechordal plate. (**B**) *Otx2* expression at 2 dpf. Red arrows indicate the brain structure. (**C**) *Fgf8* expression at 2 dpf. Upper panels show the anterior part of the embryos. White arrows indicate the anterior tip of the forebrain and red arrows indicate MHB. Lower panels show the posterior region of the embryos. Red arrows indicate the tail bud. (**D**) *MyoD* expression in somites at 34 hpf. Right panel shows the expression pattern of mildly affected P-MO-1-injected embryo. (**E**) *Krox20* expression at 34 hpf (red arrows). In control embryos, *krox20* expression was observed as two distinct domains corresponding to rhombomere 3 and 5 (left panel). In mildly affected GlcAT-P-depleted embryos (upper right) and severely affected embryos (lower right). Red arrows indicate the *krox20* expression domains in GlcAT-P-depleted embryos. (**F**) *Sox10* expression at 34 hpf (red arrows). Neural crest cells located both sides of the embryo express *sox10* in control embryos (left), in mildly affected GlcAT-P-depleted embryos (upper right), and severely affected embryos (lower right). Bars, 200 μm.

we co-injected RNA encoding Bcl-xL, a well-known inhibitor of apoptosis (Gibson et al. 1996), with P-MO-1 (Erickson et al. 1989). As a result, the injection of 250–500 pg of *Bcl-xL* RNA with P-MO-1 led to the disappearance of the dark-stained cells at both the gastrula stage and 1–2 dpf (Figure 5J–L, compare with Figure 5E–G). The blockade of the apoptosis by Bcl-xL was further confirmed by TUNEL staining (Figure 6G–I). In spite of the effective inhibition of the enhanced apoptosis, these embryos still retained the morphogenetic defects characteristic of GlcAT-P-depleted embryos such as the head hypoplasia at 2 dpf (Figure 5L). The injection of *Bcl-xL* RNA alone at both doses did not affect the development at all the stages examined. In view of these results, we thought that the ectopic apoptosis was not caused by off-targeting effects but might be caused by HNK-1 carbohydrate reduction. Therefore, we concluded that the strict regulation of HNK-1 carbohydrate expression through modulation of GlcAT-P expression is essential for organogenesis, especially in the head region, during early medaka development.

Molecular marker analysis of GlcAT-P-depleted embryos

As shown above, the most prominent phenotypic abnormality observed in GlcAT-P-depleted embryos was the head hypoplasia. To gain further insights into the cause of this defect, we performed molecular marker analyses involving in situ hybridization.

It has been well established that the induction of neural tissue requires the function of an organizer (Spemann and Mangold 1924). We thus examined the expression of chordin (chd), an established marker for the organizer. The expression of chd was detected to the same degree at mid-gastrulation (17 hpf) in both control and GlcAT-P-depleted embryos (data not shown), indicating that the functional organizer was established in the absence of GlcAT-P activity. After being specified to become the neuroectoderm, the cells in the anterior region receive signals from the prechordal plate mesendoderm, which is demarcated by goosecoid (gsc) expression, to develop into the brain structure (Cho et al. 1991). Hence, we examined the expression pattern of gsc at the late gastrulation stage (21 hpf, Figure 7A). In GlcAT-P-depleted embryos, the size of the gsc expression domain was essentially similar to that in control embryos, suggesting that the prechordal plate was properly formed in the GlcAT-P-depleted embryos.

Next, in order to examine neural patterning, the expression of otx2 which marks the central nervous system including the forebrain was investigated at the late somite stage (2 dpf). As expected from the morphological analysis shown in Figure 5, the otx2 expression domain was more greatly reduced in GlcAT-P-depleted embryos than in control ones as early as this stage, although it was not completely abolished even in the severely affected embryos (Figure 7B). The specific impairment in the formation of the brain structure was further confirmed by analyzing *fgf8* expression, which marks the anterior tip of the forebrain and the midbrain–hindbrain boundary (MHB) in the central nervous system and tail bud mesoderm. When compared with control embryos, GlcAT-P-depleted ones showed marked reduction in the *fgf8* expression domains in both the forebrain and MHB, although the expression in the tail bud was unaffected (Figure 7C).

Furthermore, we investigated if the trunk mesoderm was properly specified in GlcAT-P-depleted embryos. The expression of a notochord marker, *shh*, appeared to be unaffected even in the severely affected group of GlcAT-P-depleted embryos (data not shown). In addition, the expression of *myoD*, a marker for somite was also examined at 34 hpf (somite stage). In the embryos of the mildly affected group, *myoD* was expressed in somites as in control embryos (Figure 7D). Meanwhile, in the severely affected group, its expression was only faintly visible or undetected (data not shown). These results suggested that GlcAT-P-depleted embryos were mainly affected in the head region and most severely affected embryos were also affected in the trunk region.

Finally, we investigated the region in which HNK-1 carbohydrate expression was known to be observed. In the central nervous system, HNK-1 carbohydrate is also expressed in rhombomeres 3 and 5 (r3 and r5) in chick embryo (Kuratani 1991), both of which are demarcated by *krox20* expression (Figure 7E). As a result of examination, GlcAT-P-depleted embryos retain the *krox20* expression at 34 hpf, though the distance between r3 and r5 became shorter in mildly affected embryos at the early

somite stage (Figure 7E, upper-right panel). In severely affected embryos, however, only one domain exhibiting *krox20* expression was seen at this stage (Figure 7E, lower-right panel). Since GlcAT-P-depleted embryos showed impaired brain formation, it was unclear which rhombomere was lost. Alternatively, it is also possible that the two rhombomeres placed too close and fused with each other. Other physiologically important HNK-1 carbohydrate expressing domains are neural crest cells, shown in many species including teleost fish and mammals (Bronner-Fraser 1986; Erickson et al. 1989; Sadaghiani and Vielkind 1990). The HNK-1 carbohydrate is known to play an active role in migration of neural crest cells. For example, in the *pax6* mutant mouse, ectopically expressed HNK-1 carbohydrate perturbs migration of the midbrain neural crest cells (Nagase et al. 2001). To visualize neural crest cells, we investigated the expression of a neural crest marker, *sox10*, at the early somite stage (Figure 7F). In control embryos, *sox10* expression was observed on both lateral sides of the embryonic body at 34 hpf, whereas it was confined to one smaller region in the severely affected group of GlcAT-P-depleted embryos (Figure 7F, lower-right panel). In the embryos with milder phenotypes, two expression domains were detected as in control embryos (Figure 7F, upper-right panel). These results suggest that the proliferation and/or migration of the neural crest cells were affected, although the specification did take place in the absence of the HNK-1 carbohydrate. In addition, we performed molecular marker analyses for embryos co-injected P-MO-1 and *Bcl-xL* RNA and we obtained essentially same results compared to GlcAT-P-depleted embryos (supplementary Figure 1D and E).

Taken together, the molecular marker analyses demonstrated that the formation of the anterior neural structures, including the brain and neural crest, was compromised in GlcAT-P-depleted embryos even though the organizer and prechordal plate were properly formed. This may indicate that these defects were caused either by the proposed enhanced apoptosis of the ectodermal cells or by failure of these cells to respond properly to patterning signals released from the prechordal plate. The mesoderm in the trunk/tail region was largely unaffected in these embryos.

Discussion

In this study, we used medaka as a model organism to elucidate the function of HNK-1 in early development. We first cloned cDNAs encoding medaka GlcAT-P and GlcAT-S, which retain high sequence similarity to their human and mouse orthologs (Figure 1A and C). For *GlcAT-P*, we found two splice variants, which have not been reported in other species so far. We next examined the expression pattern of these enzymes during medaka embryogenesis. *GlcAT-P* expression was observed in a temporally restricted manner during gastrulation, followed by a second phase of expression after 2 dpf (Figure 2A and B). In contrast, *GlcAT-S* exhibited a simple expression pattern, being expressed only after 2 dpf (Figure 2A and B). The expression patterns of these two enzymes indicate that GlcAT-P, but not GlcAT-S, is the enzyme responsible for HNK-1 carbohydrate synthesis during early embryogenesis. Unfortunately, we did not obtain the significant results about the spatial expression pattern of *GlcATs* by in situ hybridization, presumably because of their low-level expression, as is true of most glycosyltransferases. We observed a few bands of HNK-1 carrier proteins as early as just after fertilization (Figure 2C). As the transcripts for both *GlcATs* were not detected before the gastrula stage, the HNK-1 carbohydrate observed at one- to two-cell stages were likely carried by maternally loaded proteins. In addition to these bands, other bands of HNK-1 carbohydrate carrier proteins appeared from 21 hpf to 2dpf although the expression level was low (Figure 2C and D).

To investigate the function of the GlcATs and HNK-1 carbohydrate during embryogenesis, we next performed gain- and loss-of-function analyses. Overproduction of the HNK-1 carbohydrate by excess GlcATs disturbed early developmental processes (Figure 3). Interestingly, the injection of *GlcAT-S* RNA had a more severe effect than *GlcAT-P* RNA. We previously reported that GlcAT-S is able to recognize the lacto-*N*-biose (Galβ1-3GlcNAc) structure as well as *N*-acetyllactosamine (Galβ1-4GlcNAc) as a terminal acceptor, while GlcAT-P strictly recognizes the *N*-acetyllactosamine structure. Therefore, this broader substrate specificity might cause more severe phenotypes observed in *GlcAT-S* RNA-injected embryos, as it would lead to more widespread overrepresentation of the HNK-1 carbohydrate on various proteins.

In loss-of-function analyses, we found that GlcAT-P is essential for proper embryogenesis, especially in the head region (Figure 5), while knockdown of GlcAT-S did not affect medaka embryonic development at all (Table I). Together, these gain- and loss-of-function analyses indicate that an appropriate level of GlcATs activity is critical for proper medaka embryogenesis. In agreement with this notion, co-injection of *GlcATs* RNA apparently could not rescue completely the phenotypic abnormalities caused by GlcAT-P depletion (data not shown).

We observed massive apoptotic cell death in the neuroectoderm of GlcAT-P-depleted embryos at the mid-gastrulation stage (Figure 7). In normal medaka embryos, apoptotic cell death becomes evident in the central nervous system and tail bud at the early somite stage (Iijima and Yokoyama 2007). Therefore, the apoptosis observed in GlcAT-P-depleted embryos is different from normal development in terms of both timing and location. Recently, it was reported that MOs injection often resulted in apoptosis in the neural region by the off-targeting effects. To eliminate this possibility, we co-injected *Bcl-xL* RNA, which is another well-known inhibitor of apoptosis (Robu et al. 2007), together with P-MO-1. With this experimental set-up, the ectopic apoptosis was almost completely blocked. However, the defects in the head morphogenesis were essentially preserved (see Figure 5L). We concluded that even though enhanced ectopic apoptosis occurs when GlcAT-P activity was depleted, there is a separate cause for the morphogenetic defect. It is well known that when cells lose the appropriate adhesion with other cells and/or extracellular matrix, they undergo apoptotic cell death (Boudreau et al. 1995; Day et al. 1999; Murray and Edgar 2000). Thus, because the HNK-1 carbohydrate is known to mainly exist on cell adhesion molecules and extracellular matrix proteins, it is possible that impaired adhesiveness of GlcAT-P-depleted cells leads to the ectopic apoptosis. In this point of view, we have tried to perform transplantation experiments (data not shown) to investigate the cause of defects in GlcAT-P-depleted embryos. From the results, we suggest that the adhesiveness or migration was

affected in GlcAT-P-depleted embryos. However, it still needs detailed examination.

In situ hybridization analyses for various differentiation markers demonstrated that depletion of *GlcAT-P* affected the formation of anterior neural structures with less disturbance of the trunk/tail region (Figure 7). As the expression of the neuroectodermal marker was reduced while a prechordal plate marker, *gsc*, was properly maintained in GlcAT-P-depleted embryos (Figure 7A), these abnormalities might be somehow caused by impaired transduction of a differentiation/maturation signal emanating from the axial mesendoderm toward the neuroectoderm. In addition, from the results of in situ hybridization with *krox20* and *sox10*, regions that were known to express the HNK-1 carbohydrate were affected, suggesting the functional importance of the HNK-1 carbohydrate in these regions.

Previously, we reported the phenotype of GlcAT-P knockout mice. The knockout mice were born with no obvious abnormalities but the adult knockout mice exhibited reduced long-term potentiation (LTP) at the Schaffer collateral-CA1 synapses and defects in spatial memory formation (Yamamoto et al. 2002). In contrast, the GlcAT-P-depleted medaka exhibited the defective head morphogenesis and enhanced apoptotic cells in early development as described above. At present, it is difficult to explain why the difference occurred. However, it is possible that another gene such as GlcAT-S might compensate for the loss of GlcAT-P activity in mouse during early development while it might not be present in medaka. In fact, GlcAT-S was not expressed in the early developmental stage in medaka (Figure 2A).

In conclusion, we identified two medaka β-1,3-glucur onyltransferases required for HNK-1 carbohydrate biosynthesis and analyzed their functions in the context of embryonic morphogenesis. Gain- and loss-of-function analyses of these two GlcATs revealed that production of an appropriate level of the HNK-1 carbohydrate is essential for proper medaka embryogenesis. The loss of GlcAT-P led us to enhance ectopic apoptosis in the neuroectoderm at the mid-gastrulation and the head region at late stages and abnormal morphogenesis in the head region. Further study is necessary to elucidate the molecular mechanisms by which loss of GlcAT-P activity leads to abnormal nervous system formation.

Materials and methods

Strain and maintenance of medaka

In the present study, all the medaka was one inbred line d-rR. Embryos were incubated at 26°C, and the developmental stages were scored as previously described (Iwamatsu 2004).

SDS–PAGE and immunoblot analysis

Staged whole embryos or tissues from adult fish were homogenized in Iwamatsu's ringer solution (Iwamatsu 1983) and then centrifuged at 17,000 × *g* for 10 min at 4°C. The precipitate was washed by being resuspended in Iwamatsu's ringer solution and centrifuged several times, and then dissolved on ice in phosphate-buffered saline (PBS) containing 0.5% SDS and protease inhibitors (Nacalai Tesque, Kyoto, Japan). Samples were sonicated and centrifuged at 17,000 × *g* for 20 min at 4°C. Proteins from each supernatant (20 μg protein for 21 hpf and 1 and 2 dpf embryos or 5 μg protein for 0, 4, and 6 dpf embryos) were resolved on a 5–20% gradient gel by SDS–PAGE (Laemmli 1970) and then transferred to nitrocellulose membranes. After blocking with 5% nonfat dried milk in Tris-buffered saline (TBS), the membranes were incubated with anti-HNK-1 antibodies (American Type Culture Collection), purified mouse myeloma IgM (ZYMED, San Francisco, CA), or anti-Myc antibodies (Calbiochem, Darmstadt, Germany), followed by horseradish peroxidase-conjugated goat anti-mouse IgM antibodies or anti-mouse IgG antibodies, respectively. Protein bands were visualized with ECL or SuperSignal West Femto and West Pico (Pierce, Rockford, IL) using a Luminoimage Analyzer LAS-3000 (Fuji, Tokyo, Japan).

Cloning of medaka GlcAT-P and GlcAT-S, and RT-PCR analysis

The sequences of degenerate primers used for the cloning were designed to cover relatively conserved regions in GlcATs of human, mouse, and fugu. RNA was prepared from medaka embryos with the TRIzol reagent (Invitrogen, Carlsbad, CA) and then reverse transcribed. PCR was then carried out using the degenerate primers designed as above to obtain partial cDNA fragments encoding proteins exhibiting sequence similarities to other vertebrate GlcATs. We then carried out 5′- and 3′-RACE using a SMART-RACE cDNA amplification kit (BD Biosciences, Franklin Lakes, NJ) according to the manufacturer's protocol, and cloned cDNAs encoding the full-length GlcAT-P and GlcAT-S proteins. Phylogenetic analysis of GlcATs was performed with a multiple alignment program ClustalW. The sequences used were hsGlcATs (*Homo sapiens*, GlcAT-P AB029396, GlcAT-S AY070019, and GlcAT-I AB009598, respectively) and mmGlcATs (*Mus musculus*, GlcAT-P AB055781, GlcAT-S AB055902, and GlcAT-I AK146264, respectively). The primer sequences used for RT-PCR analyses were (upstream and downstream): 5′-GAAGAGATATTCTTGCCATCGTACT-3′ and 5′-GAGCCAGATTCCTCTGCATC-3′ or 5′-GCAATTCCC CGAAGAGAAGAGATATTCT-3′ and 5′-GATATCTCAAA TCTCCACGTTTGGGT-3′ for GlcAT-P; 5′-GCCCTGCC GATGATCTACGCCATCA-3′ and 5′-TATGCTCGGCCACC CACAAATCCCA-3′ or 5′-TCCTCCTGCCTTGGATCCT-3′ and 5′-GGTGCTTCGCATCTCCTCAA-3′ for GlcAT-S; 5′-ACCCACACAGTGCCCATCTACGA-3′ and 5′-AGACAGCA CAGTGTTGGCGTACAG-3′ for β-actin, respectively.

Biosynthetic activity of medaka GlcATs toward the HNK-1 carbohydrate

A truncated GlcAT cDNAs lacking the start codon were amplified by PCR. The primer sequences used were: 5′-GGAATTCCCCGAAGAGAAGAGATATTC-3′ and 5′-GATATCTCAAATCTCCACGTTTGGGT-3′ for GlcAT-P; and 5′-GGAATTCCAAATCAGTGTTTTTGAGCCG-3′ and 5′-GATATCTCACACCTCGATGAGCACCG-3′ for GlcAT-S. Each sense primer contains an in-frame *Eco*RI site and each antisense primer contains an *Eco*RV site located at 3′ downstream of the stop codon. The amplified fragments were subcloned into the *Eco*RI–*Eco*RV sites of p3xFLAG-CMV-10 (Sigma-Aldrich, St Louis, MO). The plasmid was transfected into COS-1 cells on 100 mm plates using FuGene6 (Roche, Basel, Switzerland). The transfected cells were harvested for immunoblot analysis

with anti-HNK-1 antibodies (American Type Culture Collection) and anti-FLAG antibodies (Sigma-Aldrich) at 24 h after transfection.

Manipulation of medaka embryos

Capped RNAs for medaka GlcATs, EGFP, or Bcl-xL were synthesized using a RiboMAX Large Scale RNA Production System-SP6 or -T7 (Promega, Madison, WI) and purified with an RNeasy Mini kit (Qiagen, Hilden, Germany). The RNA was injected into one- to two-cell stage embryos.

For loss-of-function analyses, two different MOs for GlcAT-P and one for GlcAT-S were designed by Gene Tools, LLC (Philomath, OR). The sequences of these MOs were: P-MO-1, 5′-GAATATCTCTTCTCTTCGGCATCTC-3′; P-MO-2, 5′-TTGATCTCATCTGGAAGAGAGGAGA-3′; and S-MO, 5′-CGGCTCAAAAACACTGATTTCATGG -3′. As negative controls, MOs with a five-base mismatch were used: P-MO-1C, 5′-GAATATgTCTTgTCTTgGGgATgTC-3′; P-MO-2C, 5′-TTcATgTCATCTcGAAGAcAGcAGA-3′; and S-MO-C, 5′-CGcCTgAAAAACAgTGATTTgATcG -3′ (lower-case letters indicate the mismatched nucleotides). The MOs were diluted in Yamamoto's ringer solution (Yamamoto 1954) at 1.25 mM (P-MO-1 and -1C), 0.25 mM (P-MO-2 and -2C), or 1.0 mM (S-MO and -C), and then injected into one- to two-cell stage embryos as above.

Whole-mount in situ hybridization, immunohistochemistry, TUNEL assay and acridine orange staining

Whole-mount in situ hybridization was performed as previously described (Koshida et al. 1998). Digoxigenin-labeled RNA probes were generated in vitro with a DIG RNA Labeling Kit (SP6/T7) (Roche) or by using T3 polymerase (Applied Biosystems, Foster City, CA). The probes used in this study were *goosecoid* (MF015DA014K11), *sox10* (ensembl accession no. ENSORLG00000014587), *otx2* (AJ000939), *six3* (MF015DA006K02), *fgf8* (Ristoratore et al. 1999), and *krox20* (ensembl accession no. ENSORLG00000014600). For immunohistochemistry, staged embryos were dechorionated and fixed in PBS containing 4% paraformaldehyde overnight at 4°C, followed by incubation in PBS containing 30% sucrose. The embryos were then embedded in Tissue-Tek OCT Compound (Sakura Finetechnical, Tokyo, Japan) and immediately frozen in liquid nitrogen and stored at −80°C. Sections (5–10 μm) were made with a CM3000 cryostat (Leica Microsystems, Watzlar, Germany) and stained by anti-HNK-1 antibodies and fluorescein isothiocyanate-conjugated goat anti-mouse IgM antibodies. The stained sections were observed using a Fluoview laser confocal microscope system (Olympus, Tokyo, Japan). The TUNEL assay was performed by using a DeadEnd colorimetric detection kit (Promega) as described previously (Maroon et al. 2002). For acridine orange staining of living embryos, dechorionated embryos were washed in Iwamatsu's ringer solution and then placed in Iwamatsu's ringer solution containing 2 μg/mL acridine orange (acridinium chloride hemizinc chloride, Wako, Osaka, Japan) for 30 min at room temperature, followed by washes in Iwamatsu's ringer solution three times. The stained embryos were observed and photographed under a stereomicroscope, Leica MZ16FA, fitted with a Leica DFC 500 camera (Leica microsystems).

Funding

The Ministry of Education, Culture, Sports and Technology (16GS0313 to S.O.).

Acknowledgements

We thank Drs. Hiromu Takematsu and Masato Kinoshita for the critical discussions and comments on the manuscript. We are also grateful to Mizue Hanaki and Miwako Tonoyama for the excellent fish care. The DNA clones containing *myoD* and cDNA used in this study were generous gift from Dr. Minoru Tanaka, and the *gsc* cDNA was provided by National Institute for Basic Biology and University of Tokyo through the National Bio-Resource Project (NBRP) of the MEXT, Japan.

Abbreviations

dpf, days post-fertilization; GlcAT, glucuronyltransferase; HNK-1, human natural killer-1; hpf, hours post-fertilization; HRP, horseradish peroxidase; MO, morpholino oligonucleotides.

Supplementary data

Supplementary data for this article is available online at http://glycob.oxfordjournals.org/.

References

Boudreau N, Sympson CJ, Werb Z, Bissell MJ. 1995. Suppression of ICE and apoptosis in mammary epithelial cells by extracellular matrix. *Science.* 267:891–893.

Bronner-Fraser M. 1986. Analysis of the early stages of trunk neural crest migration in avian embryos using monoclonal antibody HNK-1. *Dev Biol.* 115:44–55.

Canning DR, Stern CD. 1988. Changes in the expression of the carbohydrate epitope HNK-1 associated with mesoderm induction in the chick embryo. *Development.* 104:643–655.

Cho KW, Blumberg B, Steinbeisser H, De Robertis EM. 1991. Molecular nature of Spemann's organizer: The role of the Xenopus homeobox gene goosecoid. *Cell.* 67:1111–1120.

Chou DK, Ilyas AA, Evans JE, Costello C, Quarles RH, Jungalwala F B. 1986. Structure of sulfated glucuronyl glycolipids in the nervous system reacting with HNK-1 antibody and some IgM paraproteins in neuropathy. *J Biol Chem.* 261:11717–11725.

Day ML, Zhao X, Vallorosi CJ, Putzi M, Powell CT, Lin C, Day KC. 1999. E-cadherin mediates aggregation-dependent survival of prostate and mammary epithelial cells through the retinoblastoma cell cycle control pathway. *J Biol Chem.* 274:9656–9664.

Gibson L, Holmgreen SP, Huang DC, Bernard O, Copeland NG, Jenkins NA, Sutherland GR, Baker E, Adams JM, Cory S. 1996. bcl-w, a novel member of the bcl-2 family, promotes cell survival. *Oncogene.* 13:665–675.

Erickson CA, Loring JF, Lester SM. 1989. Migratory pathways of HNK-1-immunoreactive neural crest cells in the rat embryo. *Dev Biol.* 134:112–118.

Iijima N, Yokoyama T. 2007. Apoptosis in the medaka embryo in the early developmental stage. *Acta Histochem Cytochem.* 40:1–7.

Iwamatsu T. 1983. A new technique for dechorination and observations on the development of the naked egg in Oryziaslatipes. *J. Exp. Zool.* 228:83–89.

Iwamatsu T. 2004. Stages of normal development in the medaka Oryzias latipes. *Mech Dev.* 121:605–618.

Kakuda S, Shiba T, Ishiguro M, Tagawa H, Oka S, Kajihara Y, Kawasaki T, Wakatsuki S, Kato R. 2004. Structural basis for acceptor substrate recognition of a human glucuronyltransferase, GlcAT-P, an enzyme

critical in the biosynthesis of the carbohydrate epitope HNK-1. *J Biol Chem.* 279:22693–22703.

Kitagawa H, Tone Y, Tamura J, Neumann KW, Ogawa T, Oka S, Kawasaki T, Sugahara K. 1998. Molecular cloning and expression of glucuronyltransferase I involved in the biosynthesis of the glycosaminoglycan-protein linkage region of proteoglycans. *J Biol Chem.* 273:6615–6618.

Koshida S, Shinya M, Mizuno T, Kuroiwa A, Takeda H. 1998. Initial anteroposterior pattern of the zebrafish central nervous system is determined by differential competence of the epiblast. *Development.* 125:1957–1966.

Kuratani SC. 1991. Alternate expression of the HNK-1 epitope in rhombomeres of the chick embryo. *Dev Biol.* 144:215–219.

Laemmli UK. 1970. Cleavage of structural proteins during the assembly of the head of bacteriophage T4. *Nature.* 227:680–685.

Liedtke S, Geyer H, Wuhrer M, Geyer R, Frank G, Gerardy-Schahn R, Zähringer U, Schachner M. 2001. Characterization of *N*-glycans from mouse brain neural cell adhesion molecule. *Glycobiology.* 11:373–384.

Lowe JB, Marth JD. 2003. A genetic approach to mammalian glycan function. *Annu Rev Biochem.* 72:643–691.

Maroon H, Walshe J, Mahmood R, Kiefer P, Dickson C, Mason I. 2002. Fgf3 and Fgf8 are required together for formation of the otic placode and vesicle. *Development.* 129:2099–2108.

Metzler M, Gertz A, Sarkar M, Schachter H, Schrader JW, Marth JD. 1994. Complex asparagine-linked oligosaccharides are required for morphogenic events during post-implantation development. *Embo J.* 13:2056–2065.

Mitsumoto Y, Oka S, Sakuma H, Inazawa J, Kawasaki T. 2000. Cloning and chromosomal mapping of human glucuronyltransferase involved in biosynthesis of the HNK-1 carbohydrate epitope. *Genomics.* 65:166–173.

Murray P, Edgar D. 2000. Regulation of programmed cell death by basement membranes in embryonic development. *J Cell Biol.* 150:1215–1221.

Nagase T, Nakamura S, Harii K, Osumi N. 2001. Ectopically localized HNK-1 epitope perturbs migration of the midbrain neural crest cells in Pax6 mutant rat. *Dev Growth Differ.* 43:683–692.

Negishi M, Dong J, Darden TA, Pedersen LG, Pedersen LC. 2003. Glucosaminylglycan biosynthesis: What we can learn from the X-ray crystal structures of glycosyltransferases GlcAT1 and EXTL2. *Biochem Biophys Res Commun.* 303:393–398.

Ohtsubo K, Marth JD. 2006. Glycosylation in cellular mechanisms of health and disease. *Cell.* 126:855–867.

Ristoratore F, Carl M, Deschet K, Richard-Parpaillon L, Boujard D, Wittbrodt J, Chourrout D, Bourrat F, Joly JS. 1999. The midbrain–hindbrain boundary genetic cascade is activated ectopically in the diencephalon in response to the widespread expression of one of its components, the medaka gene Ol-eng2. *Development.* 126:3769–3779.

Robu ME, Larson JD, Nasevicius A, Beiraghi S, Brenner C, Farber SA, Ekker SC. 2007. p53 activation by knockdown technologies. *PLoS Genet.* 3:e78.

Sadaghiani B, Vielkind JR. 1990. Distribution and migration pathways of HNK-1-immunoreactive neural crest cells in teleost fish embryos. *Development.* 110:197–209.

Saghatelyan AK, Gorissen S, Albert M, Hertlein B, Schachner M, Dityatev A. 2000. The extracellular matrix molecule tenascin-R and its HNK-1 carbohydrate modulate perisomatic inhibition and long-term potentiation in the CA1 region of the hippocampus. *Eur J Neurosci.* 12:3331–3342.

Schwarting GA, Jungalwala FB, Chou DK, Boyer AM, Yamamoto M. 1987. Sulfated glucuronic acid-containing glycoconjugates are temporally and spatially regulated antigens in the developing mammalian nervous system. *Dev Biol.* 120:65–76.

Seiki T, Oka S, Terayama K, Imiya K, Kawasaki T. 1999. Molecular cloning and expression of a second glucuronyltransferase involved in the biosynthesis of the HNK-1 carbohydrate epitope. *Biochem Biophys Res Commun.* 255:182–187.

Shiba T, Kakuda S, Ishiguro M, Morita I, Oka S, Kawasaki T, Wakatsuki S, Kato R. 2006. Crystal structure of GlcAT-S, a human glucuronyltransferase, involved in the biosynthesis of the HNK-1 carbohydrate epitope. *Proteins.* 65:499–508.

Solter D, Knowles BB. 1978. Monoclonal antibody defining a stage-specific mouse embryonic antigen (SSEA-1). *Proc Natl Acad Sci USA.* 75:5565–5569.

Spemann H, Mangold H. 1924. Uber Induktion von Embryonalanlagen durch Implantation artfremder Organisatoren. *Roux's Arch. Dev. Biol.* 100:599–638.

Stern CD, Canning DR. 1990. Origin of cells giving rise to mesoderm and endoderm in chick embryo. *Nature.* 343:273–275.

Terayama K, Oka S, Seiki T, Miki Y, Nakamura A, Kozutsumi Y, Takio K, Kawasaki T. 1997. Cloning and functional expression of a novel glucuronyltransferase involved in the biosynthesis of the carbohydrate epitope HNK-1. *Proc Natl Acad Sci USA.* 94:6093–6098.

Terayama K, Seiki T, Nakamura A, Matsumori K, Ohta S, Oka S, Sugita M, Kawasaki T. 1998. Purification and characterization of a glucuronyltransferase involved in the biosynthesis of the HNK-1 epitope on glycoproteins from rat brain. *J Biol Chem.* 273:30295–30300.

Voshol H, Van Zuylen CW, Orberger G, Vliegenthart JF, Schachner M. 1996. Structure of the HNK-1 carbohydrate epitope on bovine peripheral myelin glycoprotein P0. *J Biol Chem.* 271:22957–22960.

Yamamoto S, Oka S, Saito-Ohara F, Inazawa J, Kawasaki T. 2002. Molecular cloning and genomic analysis of mouse glucuronyltransferase involved in biosynthesis of the HNK-1 epitope. *J Biochem.* 131:337–347.

Yamamoto T. 1954. Physiological studies on fertilization and activation of fish eggs: V. The role of calcium ions in activation of Oryzias eggs. *Exp Cell Res.* 6:56–68.

Yoshihara Y, Oka S, Watanabe Y, Mori K. 1991. Developmentally and spatially regulated expression of HNK-1 carbohydrate antigen on a novel phosphatidylinositol-anchored glycoprotein in rat brain. *J Cell Biol.* 115:731–744.

MECHANISMS OF DEVELOPMENT 126 (2009) 580–594

available at www.sciencedirect.com

ScienceDirect

journal homepage: www.elsevier.com/locate/modo

MECHANISMS OF DEVELOPMENT

Essential role of beta-1,4-galactosyltransferase 2 during medaka (*Oryzias latipes*) gastrulation

Yasuhiro Tonoyama[a,d], *Daisuke Anzai*[a], *Atsushi Ikeda*[a], *Shinako Kakuda*[d], *Masato Kinoshita*[b], *Toshisuke Kawasaki*[c], *Shogo Oka*[d,*]

[a]*Department of Biological Chemistry, Graduate School of Pharmaceutical Sciences, Kyoto University, Kyoto 606-8501, Japan*
[b]*Division of Applied Biosciences, Graduate School of Agriculture, Kyoto University, Kyoto 606-8502, Japan*
[c]*Research Center for Glycobiotechnology, Ritsumeikan University, Shiga, Japan*
[d]*Department of Biological Chemistry, Human Health Sciences, Graduate School of Medicine, Kyoto University, 53 Kawahara-cho, Shogoin, Sakyo-ku, Kyoto 606-8507, Japan*

ARTICLE INFO

Article history:
Received 6 October 2008
Received in revised form
11 March 2009
Accepted 12 March 2009
Available online 24 March 2009

Keywords:
Medaka
Glycosyltransferase
Glycan
β-1,4-Galactosyltransferase 2
Convergence and extension
Mediolateral cell intercalation
Morphogenesis
Gastrulation
Embryogenesis

ABSTRACT

Glycans are known to play important roles in vertebrate development; however, it is difficult to analyze in mammals because it takes place *in utero*. Therefore, we used medaka (*Oryzias latipes*) to clarify the roles of glycans during vertebrate development. β-1,4-Galactosyltransferase is one of the key enzymes in the biosynthesis of the lactosamine structures that are commonly found on glycoproteins and glycolipids. Here, we show the essential role of β4GalT2 during medaka development. Depletion of β4GalT2 by morpholino antisense oligonucleotide injection resulted in significant morphological defects, such as shortening of the anterior–posterior axis, cyclopia, impaired somite segmentation, and head hypoplasia. *In situ* hybridization analyses revealed that the loss of β4GalT2 led to defective anterior–posterior axis elongation during gastrulation without affecting organizer formation. Furthermore, a cell tracing experiment demonstrated that β4GalT2 knockdown mainly affects mediolateral cell intercalation, which contributes to anterior–posterior axis elongation. A cell transplantation experiment indicated that glycans are produced by β4GalT2 cell-autonomously during gastrulation. β4GalT2 depletion also led to enhanced apoptosis; however, this does not account for the phenotypic abnormalities, as blockade of apoptosis failed to compensate for the β4GalT2 depletion. Our data suggest that β4GalT2 activity is cell-autonomously required in cells undergoing mediolateral cell intercalation, which drives extension movements during medaka gastrulation.

1. Introduction

Glycosylation is a major post-translational modification that regulates the functions of proteins involved in various biological events including embryogenesis. Several studies using glycosyltransferase-deficient mice have demonstrated the important roles of glycans in early mammalian development (Lowe and Marth, 2003). For example, N-acetylglucosaminyltransferase 1 (*Mgat1*)-deficient mice develop morphogenic abnormalities by embryonic day (E) 9.5 and fail to survive beyond E10.5 (Campbell et al., 1995). Additionally, UDP-GlcNAc: dolichol phosphate N-acetylglucosamine-1-phosphate transferase (GPT) deficient mice, which completely lack N-glycans, die shortly after implantation with apparent

* Corresponding author. Tel./fax: +81 75 751 3959.
E-mail address: shogo@hs.med.kyoto-u.ac.jp (S. Oka).
0925-4773/$ - see front matter
doi:10.1016/j.mod.2009.03.004

cell degeneration among both embryonic and extraembryonic cell types (Marek et al., 1999). These lines of evidence indicate that the N-glycans present on proteins are required for mammalian embryogenesis. Indeed, in humans, genetic diseases, the so-called congenital disorders of glycosylation (CDG), have been reported, in which a mutation in one of the glycosyltransferase genes causes morphological and functional abnormalities during embryogenesis and organogenesis (Grunewald et al., 2002). In mammals, however, it is difficult to analyze early developmental processes in detail, because they take place in the uterus; therefore, we used medaka (*Oryzias latipes*), a teleost fish that is a good model of vertebrate development, to clarify the roles of glycans, especially in early development.

Convergence and extension movements are key cell movements in vertebrate morphogenesis. These movements are defined as a combination of cell migration toward the dorsal midline (convergence) and body axis elongation (extension), and are essential for sculpting the body plan during vertebrate gastrulation. The cooperation of a variety of cell movements, including directed migration, mediolateral cell intercalation, and cell shape changes, is required for the execution of convergence and extension movements (Solnica-Krezel, 2005). Zebrafish and *Xenopus* embryos in which these movements have been disrupted exhibit significant morphological abnormalities, such as a shortened body axis and cyclopia. Genetic analyses of these mutants have revealed the requirement of various molecules in these movements, such as the Fgf and Wnt/PCP signaling pathway components (Heisenberg et al., 2000; Kilian et al., 2003; Shimada et al., 2008; Tada and Smith, 2000; Topczewski et al., 2001) and cell adhesion molecules (Kim et al., 1998; McFarland et al., 2005; Yamamoto et al., 1998).

The N-acetyllactosamine structure (Galβ1-4GlcNAc-R) is commonly found in N-linked and O-linked glycans of glycoproteins as well as in glycolipids. It is known to be involved in galectin-mediated biological events including apoptosis and is an active carbohydrate determinant involved in cell adhesion processes (Taylor and Drickamer, 2007). β-1,4-Galactosyltransferase (β4GalT), which catalyzes the transfer of Gal from the nucleotide sugar UDP-Gal to the acceptor sugar GlcNAc, is one of the key enzymes in the biosynthesis of this N-acetyllactosamine structure. Seven human genes that encode proteins with β4GalT activity have been cloned so far (Lo et al., 1998). As mentioned above, N-glycosylation of proteins is essential for mammalian early development. Thus, we have focused on the β4GalT involved in the biosynthesis of N-glycan on proteins. It is known that β4GalT1, β4GalT2, and β4GalT5 are responsible for the biosynthesis of most N-glycans in mammals (Almeida et al., 1997; Sato et al., 1998). In spite of the importance of its galactosyltransferase activity for producing glycans that contain the N-acetyllactosamine structure on proteins, *β4GalT1* deficient mice can survive beyond birth and possess residual N-acetyllactosamine structures in their N-glycan (Kido et al., 1998; Lu et al., 1997). These results suggest that another β4GalT, rather than β4GalT1, is involved in the regulation of early development.

In this study, we focused on the role of β4GalT2 during development, which has a similar substrate specificity to that of β4GalT1. Depletion of β4GalT2 by injection of morpholino antisense oligonucleotides into medaka embryos led to significant morphological defects, such as shortening of the anterior–posterior axis, cyclopia, impaired segmentation of somites, and hypoplasia of the head. We also found that these phenotypes were mainly caused by defects in the extension movement during gastrulation. Cell tracing and transplantation experiments revealed that β4GalT2 activity is cell-autonomously required in cells undergoing mediolateral cell intercalation. Finally, we demonstrated that although depletion of β4GalT2 leads to enhanced apoptotic cell death during early development, this does not fully account for the morphological defects described above, as the blockade of the apoptosis by Bcl-xL failed to rescue them.

2. Results

2.1. *Molecular cloning and phylogenetic analysis of medaka β4GalT2*

To address the roles of β-1,4-galactosyltransferase 2 (β4GalT2) in medaka development, we first cloned a cDNA encoding full-length medaka β4GalT2 (olβ4GalT2, Genbank Accession No. AB282995). Medaka β4GalT2 showed amino acid identities of 90.6%, 68.7%, and 66.1% with fugu (*Takifugu rubripes*), human, and mouse orthologs, respectively. Multiple sequence alignment analysis with ClustalW revealed that medaka β4GalT2 contains several sequence motifs that are conserved among β4GalT (Lo et al., 1998), such as a putative transmembrane domain (Fig. 1A, red letters), ENRA, N(V/I)G, DVD, and WGWGGEDDD (Fig. 1A, red boxes). The position of Cys residues was also conserved among medaka β4GalT2 and the aforementioned orthologs (Fig. 1A, yellow boxes). To further confirm that the cloned cDNA encodes a β4GalT2 ortholog, we carried out phylogenetic analysis and found that medaka β4GalT2 showed higher similarity to β4GalT2 than to any other human β4GalT (Fig. 1B). The amino acid identity of medaka β4GalT2 to human β4GalT1, 3, and 4–7 was 49.7%, 52.6%, 45.5%, 44.4%, 36.4%, and 29.4%, respectively. These results indicate that the cDNA cloned here from medaka is a bona fide ortholog of mammalian β4GalT2.

2.2. *The spatiotemporal expression pattern of β4GalT2 during early development*

The temporal expression pattern of *β4GalT2* mRNA during early development was determined by quantitative RT-PCR (Fig. 2A). Strong expression was found in embryos at the 1-cell stage, indicating that the *β4GalT2* mRNA was maternally loaded, and the expression level gradually decreased up to the bud stage and then slightly increased at the 2-somite stage. At 5 days post-fertilization (dpf), even higher expression was found than in the 1-cell stage embryos (data not shown). Next, the spatial expression pattern of *β4GalT2* was determined by whole-mount *in situ* hybridization. We used a probe against the most divergent region among the β4GalT family members to minimize the possible cross-hybridization with mRNA encoding other *β4GalT*. *β4GalT2* was ubiquitously expressed in blastulae to 95% epiboly embryos (Fig. 2B–E). At the 12-somite stage, the expression was concentrated in the

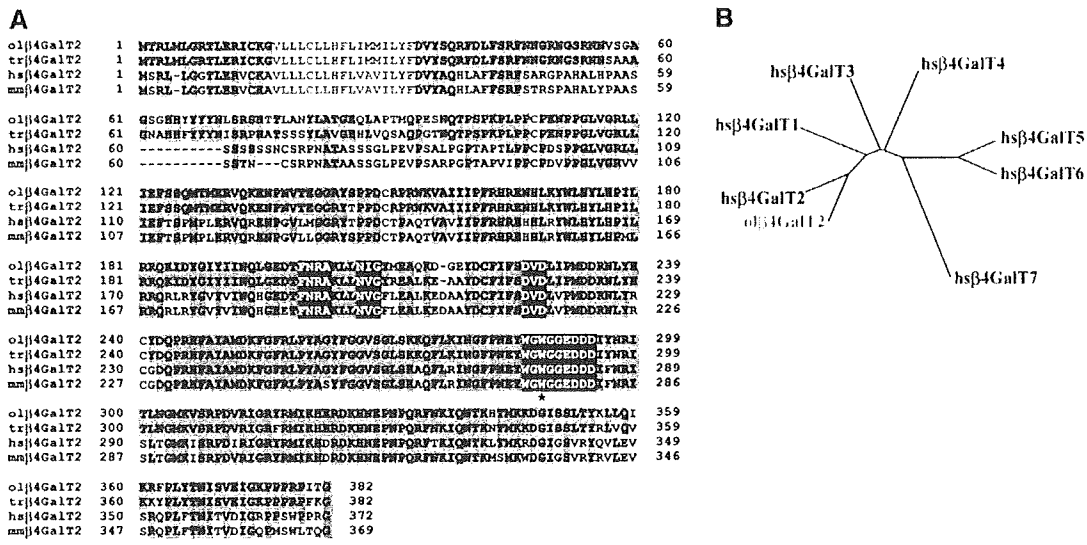

Fig. 1 – Alignment and phylogenetic analysis of medaka β4GalT2. (A) The alignment of the medaka β4GalT2 (olβ4GalT2) amino acid sequence with those of fugu β4GalT2 (trβ4GalT2), human β4GalT2 (hsβ4GalT2), and mouse β4GalT2 (mmβ4GalT2). Identical amino acid residues are boxed in blue. Red letters indicate a putative transmembrane domain (amino acids 17–33), and red boxes indicate short sequence motifs, FNRA, N (V/I) G, DVD, WGWGGEDDD, that are commonly found in the β4GalT family. Yellow boxes indicate the positions of cysteine residues that are conserved among these enzymes. The asterisk indicates a tryptophan residue that has been substituted by site-directed mutagenesis. (B) A phylogenetic dendrogram of β4GalT, constructed using ClustalW. Medaka β4GalT2 has the highest similarity to β4GalT2 among the human β4GalT.

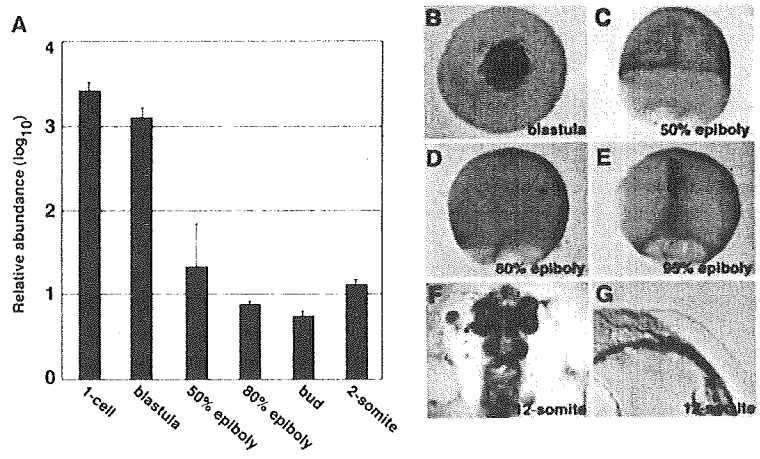

Fig. 2 – The spatiotemporal expression pattern of *β4GalT2* during early medaka development. (A) Relative expression levels were determined by quantitative RT-PCR for *β4GalT2*. Data were normalized with *β-actin* at each stage and presented on a log scale. The error bars represent SD. The expression level of *β4GalT2* gradually decreased up to the bud stage and then increased at the 2-somite stage. (B–G) Whole-mount *in situ* hybridization analysis of *β4GalT2* expression. *β4GalT2* mRNA was ubiquitously detected at the blastula (B), 50% epiboly (C), 80% epiboly stages (D) and 95% epiboly stage (E). At the 12-somite stage, the expression was markedly confined to the eyes and the brain (F), whereas it was observed weakly or absent in the trunk and tail (G). (B) Animal pole view; (C–F) dorsal view, animal pole is to the top; (G) lateral view, dorsal is to the top.

midbrain, the hindbrain, and the developing eyes (Fig. 2F). In the trunk/tail region, however, the expression was weak or almost absent (Fig. 2G). *In situ* hybridization with a sense probe targeting the same region of *β4GalT2* gave no signal at any stage (data not shown).

2.3. *Severe morphological abnormalities in β4GalT2-depleted embryos*

To address the roles of β4GalT2 in medaka early development, we employed a loss-of-function strategy. We designed

a morpholino antisense oligonucleotide against *β4GalT2* mRNA (*β4GalT2* MO) and injected it into medaka embryos at the 1-cell stage. As a control, we used a morpholino oligonucleotide containing a five-base mismatch to the target site (control MO). The injection of the control MO did not lead to any obvious abnormalities (Fig. 3A, E, I, M, 96% normal, $n = 100$). At 2 dpf, a shortened anterior–posterior axis with hypoplasia of the head was observed (Fig. 3B and F, 86% with abnormalities, $n = 100$), and the segmentation of somites was also severely impaired in embryos injected with *β4GalT2* MO (Fig. 3J). At 3 dpf, cyclopia was observed in *β4GalT2* MO-injected embryos (Fig. 3N), whereas two eyes were evident in the control MO-injected embryos (Fig. 3M), suggesting that the splitting of the eye field was defective in the β4GalT2-depleted embryos. In addition, malformation of the heart and blood vessels was seen at the same stage (compare Fig. 3M and N; arrows in Fig. 3M indicate the heart and blood vessels). These morphological abnormalities were also observed in embryos injected with another morpholino antisense oligonucleotide, *β4GalT2* MO2, which has no sequence overlap with *β4GalT2* MO (data not shown). To assess the antisense effect of *β4GalT2* MO on galactosyltransferase activity, we measured the activity toward a glycoprotein acceptor in control MO- and *β4GalT2* MO-injected embryos. At the bud stage, the activity was decreased by 56% in the *β4GalT2* MO-injected embryos compared to that in the control embryos (control MO: 1.68 pmol/h/embryo; β4GalT2 MO: 0.94 pmol/h/embryo, Fig. S1).

To further confirm the specificity of *β4GalT2* MO, we performed a complementation analysis using medaka *β4GalT2* RNA. As expected, the phenotypic abnormalities observed in the *β4GalT2* MO-injected embryos were almost completely rescued by co-injection of medaka *β4GalT2* RNA, which lacks a binding site for *β4GalT2* MO around the start codon (Fig. 3C, G, K, O, 28% with abnormalities, $n = 100$). Interestingly, co-injection of RNA encoding the mutant *β4GalT2*-W288A (Fig. 1A, asterisk), which lacks enzymatic activity (Ramasamy et al., 2003), failed to rescue the abnormalities (Fig. 3D, H, L, P, 90% with abnormalities, $n = 40$). This indicates that the β-1,4-galactosyltransferase activity of β4GalT2 is required for morphogenesis in medaka embryos. Taken together, these results suggest that the glycan(s) biosynthesized by β4GalT2 are necessary for proper patterning of medaka embryos during early development.

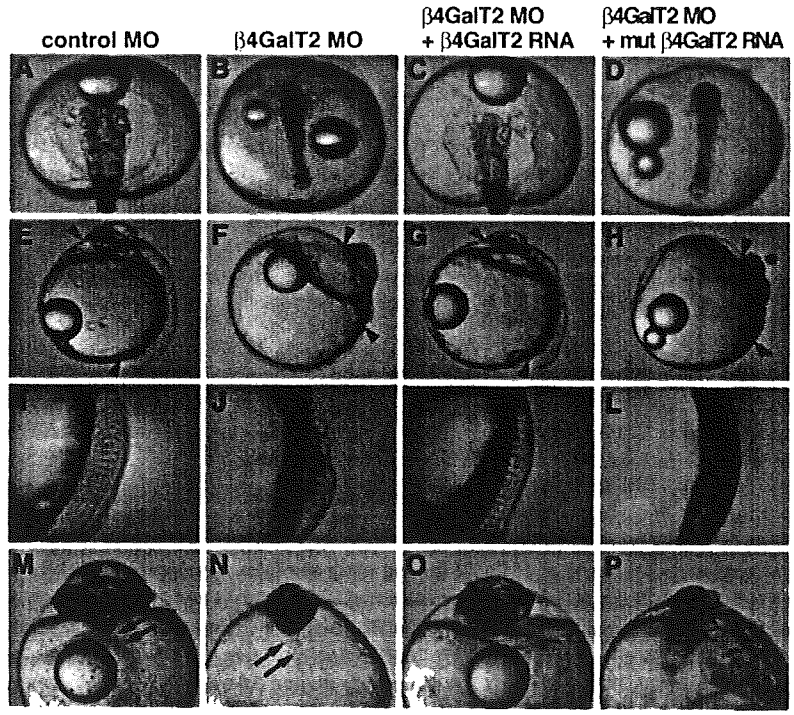

Fig. 3 – β4GalT2-depletion affects proper morphogenesis in medaka embryos. (A, E, I, M) The injection of control MO containing a five-base mismatch did not lead to any obvious phenotype (96% normal, $n = 100$). (B, F, J, N) Embryos injected with *β4GalT2* MO displayed a shortened anterior–posterior axis (arrow heads) with hypoplasia of the head, cyclopia, no segmentation of somites, malformation of blood vessels and the heart at the 15-somite stage (86% with abnormalities, $n = 100$, compare panels M and N, arrows). (C, G, K, O) The phenotypic abnormalities observed in the *β4GalT2* MO-injected embryos were rescued by co-injection of wild-type *β4GalT2* RNA (200 pg) (28% with abnormalities, $n = 100$). (D, H, L, P) The co-injection of mut *β4GalT2* RNA, which encodes a mutant protein that lacks enzymatic activity, failed to rescue the abnormality (90% with abnormalities, $n = 40$). (A–D) Dorsal view, animal pole to the top; (E–L) lateral view, the arrowheads denote the anterior and posterior ends of the embryonic body. Dorsal is to the right; (M–P) frontal view; (A–L) 15-somite stage; (M–P) 3 dpf.

2.4. *The essential role of β4GalT2 during medaka gastrulation*

In order to analyze the abnormalities observed in β4GalT2-depleted embryos in more detail, we first observed the morphology of both the control and *β4GalT2* MO-injected embryos during gastrulation, which is the most critical process for morphogenesis in early development. At the 30% epiboly stage (shield stage), the embryonic shield formed normally in the *β4GalT2* MO-injected embryos as it did in the control MO-injected embryos (Fig. 4A and F, black arrows). The movements of epiboly, which drive cells vegetally, also occurred normally in the *β4GalT2* MO-injected embryos (compare Fig. 4A–D with F–I, white arrowheads). At the 95% epiboly stage (the late gastrula stage), however, the *β4GalT2* MO-injected embryos became much thinner than the control MO-injected embryos (Fig. 4D and I, bar). At the bud stage, shortening of the embryonic body along the anterior–posterior axis was apparent (Fig. 4E and J, black arrowheads). These results indicate that *β4GalT2* MO-injected embryos start to exhibit abnormal characteristics at late gastrulation.

We next carried out whole-mount *in situ* hybridization for various marker genes associated with early development. At the early gastrula stage, *no tail* (*ntl*) and *spadetail* (*spt*), panmesodermal markers, were expressed normally in the both control and *β4GalT2* MO-injected embryos (Fig. 5A and B). Moreover, the expression of the two organizer marker genes *chordin* (*chd*) and *goosecoid* (*gsc*), and that of epidermis marker gene *bmp2* were unaffected (Fig. 5C–E). These results suggest that the mesoderm was properly induced and that the functional organizer was established in the *β4GalT2* MO-injected embryos. The shape and size of the *gsc* and *chd* expression domains were indistinguishable between the control and *β4GalT2* MO-injected embryos, indicating that prospective axial mesodermal cells were present normally in the β4GalT2-depleted embryos at the shield stage. At the segmentation stage, the *gsc* expression domain, which demarcates the prechordal mesendoderm (prospective prechordal plate), was observed in both the *β4GalT2* MO-injected and the control MO-injected embryos (Fig. 5F), although the area of the *gsc* expression domain was smaller in the *β4GalT2* MO-injected embryos than in the control MO-injected embryos at this stage. Notably, the ntl expression domain, which represents the chordamesoderm and tail bud mesoderm at this stage, was antero-posteriorly shorter and significantly disrupted in the *β4GalT2* MO-injected embryos (Fig. 5G). The expression of spt, which marks the tail bud mesoderm at this stage, was expanded in the *β4GalT2* MO-injected embryos (Fig. 5H). Next, we examined the expression of the paraxial mesodermal markers *papc* and *myoD*. However, we failed to detect these markers at the segmentation stage in the *β4GalT2* MO-injected embryos (data not shown). We therefore examined the expression of *dlx3*, which marks the boundary between the neural and epidermal ectoderms and found that the width of the neuroectodermal region was mediolaterally broader in the *β4GalT2* MO-injected embryos than that of the control embryos at the 90% epiboly stage (Fig. 5I); however, at the bud stage, the broadened width observed in the *β4GalT2* MO-injected embryos had narrowed to a similar level to that in the control embryos, while the length along the anterior-posterior axis of the *dlx3* expression domain was shortened in the *β4GalT2* MO-injected embryos (Fig. 5J). As shown in Fig 5K and L, we examined the expression of *sox17α*, an early endoderm marker. At the 80% epiboly stage, the expression in the control embryos was similar to that in β4GalT2-depleted embryos (Fig. 5K), but was significantly decreased in the β4GalT2-depleted embryos at the 90% epiboly stage (Fig. 5L) and bud stage (data not shown). At the segmentation stage, the expression of *six3* (forebrain marker) was detected in the β4GalT2-depleted embryos (Fig. 5M), and the expression of *pax2* (midbrain–hindbrain boundary marker) was reduced significantly or absent at the same stage (Fig. 5N). In summary, at early gastrulation, cell fate specification occurred normally in the β4GalT2-depleted embryos; however, defective expression patterns clearly appeared in these embryos just before the segmentation stage, suggesting

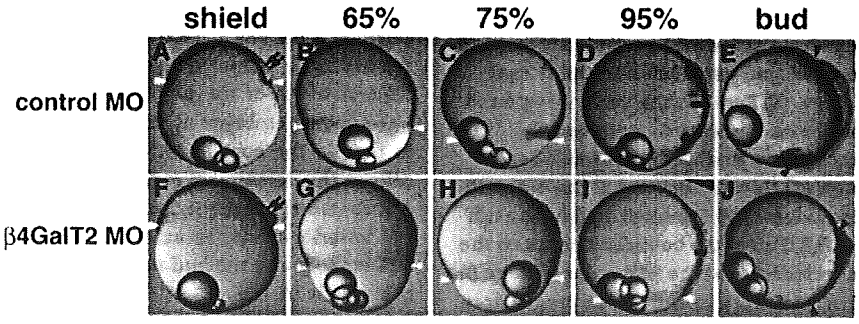

Fig. 4 – Abnormal morphogenesis of β4GalT2-depleted embryos during gastrulation. (A–E) Embryos injected with control MO. Typical embryos are shown at all stages. (F–J) Embryos injected with *β4GalT2* MO; animal pole is to the top, and dorsal is to the right. Sixty-five percent, 75%, and 95% indicate 65%, 75%, and 95% epiboly stage, respectively. The white arrowheads indicate the edge of the blastoderm. At the shield stage, the embryonic shield formed normally in the *β4GalT2* MO-injected embryos (compare A and F, arrows). Epiboly movements, which drive cells vegetally, also occurred normally in the *β4GalT2* MO-injected embryos (A–D and F–I, white arrowheads). Early morphogenetic abnormalities were observed at the late gastrula stage. The black bars in panels (D) and (I) represent the dorsoventral width of the embryonic body. Abnormalities were apparent at the bud stage (E, J, black arrowheads).

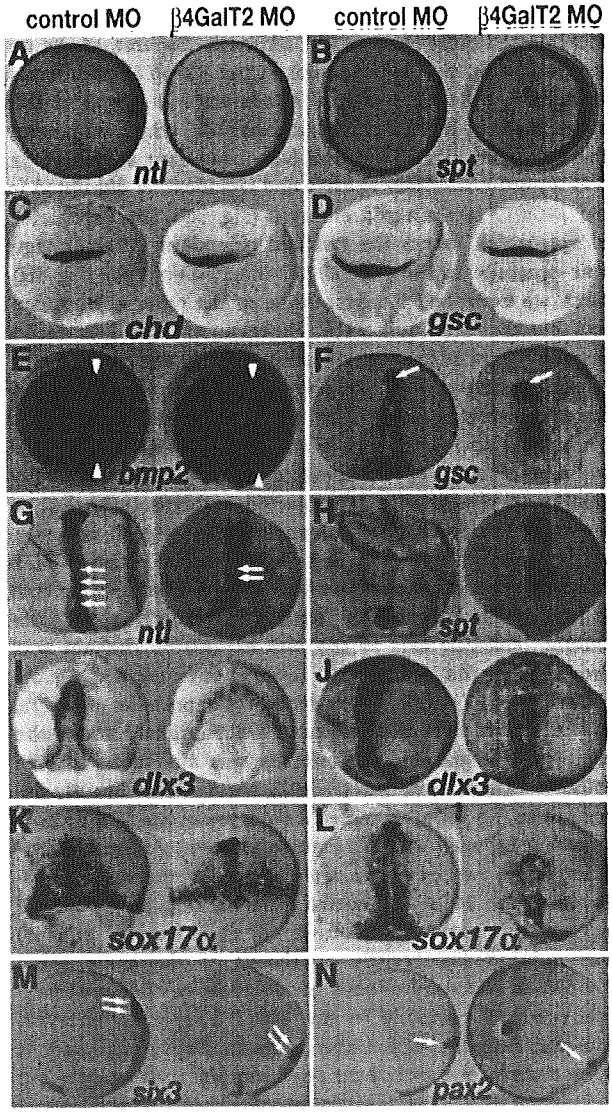

Fig. 5 – Marker gene expression in β4GalT2-depleted embryos. (A,B) *No tail/brachyury* (*ntl*) and *spadetail* (*spt*) expression in the mesoderm at the mid-gastrula stage. (C,D) *Chordin* (*chd*) and *goosecoid* (*gsc*) expression in the dorsal region at the shield stage. (E) *Bmp2* in the ventral region at the shield stage (arrowheads indicate dorsal-ventral boundary). (F) *Goosecoid* in the prechordal mesendoderm (arrow) at the bud stage. (G) *No tail/brachyury* at the 4-somite stage in the chordamesoderm. (H) *Spadetail* (*spt*) in the tail bud at 4-somite stage. (I,J) *Dlx3* at the boundary between the neural and epidermal ectoderms at the 90% epiboly stage (I) and the bud stage (J). (K,L) *Sox17α* in endoderm progenitors at the 70% epiboly stage (K) and the 90% epiboly stage (L), respectively. (M,N) *Six3* in the forebrain and *pax2* at the midbrain–hindbrain boundary during the bud stage. Expression of mRNA was detected by whole-mount *in situ* hybridization. (A, B, E) Animal pole view, dorsal is to the right; (C,D,F–L) dorsal view, animal pole is to the top; (M, N) lateral view, animal pole is to the top, and dorsal is to the right.

that β4GalT2 activity is essential for cellular events, such as cell movement and/or apoptosis in late gastrulae.

2.5. *The requirement of β4GalT2 for the extension movements mediated by mediolateral cell intercalation during late medaka gastrulation*

Multiple cell movements occur coordinately during vertebrate gastrulation (Solnica-Krezel, 2005). In zebrafish gastrulae, directed cell migration toward the dorsal midline takes place in the lateral regions of the gastrulae, while mediolateral cell intercalation occurs in the dorsal region (Myers et al., 2002). In zebrafish, the convergence and extension movements or mediolateral cell intercalation during gastrulation are impaired in most embryos that show a shortened anterior-posterior axis and cyclopia, despite normal dorsoventral patterning (Heisenberg et al., 2000; Kilian et al., 2003; Topczewski et al., 2001). To study whether β4GalT2 affects cell movements during gastrulation, we performed a cell tracing experiment in medaka embryos using DMNB-caged fluorescein dextran (Kozlowski et al., 1997; Sepich et al., 2000). Caged fluorescent dye was injected with either *β4GalT2* MO or control MO into 1-cell stage embryos. At the shield stage, a population of cells was marked by UV-mediated uncaging, and the changes in their location were traced during gastrulation. When the cells in the lateralmost region were marked, normal directed dorsal migration of labeled cells was observed in the control MO-injected embryos (Fig. 6A–C). In the *β4GalT2* MO-injected embryos, the labeled cells failed to distribute anteriorly along the elongating anterior–posterior axis, although directed dorsal migration did take place (Fig. 6D–F). These abnormal cell motilities are probably due to reduced mediolateral cell intercalation (see below). When examined in more detail by measuring the angle between the dorsal midline and the marked cells, a delay in dorsal migration was seen in the *β4GalT2* MO-injected embryos at the 80% epiboly and the bud stage, but the differences were not significant, suggesting that directed dorsal migration is normal in the *β4GalT2* MO-injected embryos (Fig. 6G). Consistent with this finding, the mediolateral width of the expression domains of six3 and pax2 in the *β4GalT2* MO-injected embryos at the segmentation stage were not broad compared to those in the control MO-injected embryos (Fig. S2A and B). The mediolateral width of the expression domain of dlx3 in *β4GalT2* MO-injected embryos at the bud stage was also comparable to that in the control MO-injected embryos (Fig. 5J). When cells in the dorsalmost region were marked, the labeled cells distributed throughout the midline as a narrow stripe along the anterior–posterior axis in the control embryos at both 80% epiboly and the bud stage (Fig. 6H–J). In contrast, the labeled cells in the *β4GalT2* MO-injected embryos were scattered across a broader region along the anterior–posterior axis (Fig. 6K–M). These observations indicate that β4GalT2 is necessary for extension movement. To investigate the effect on extension movement, the distribution of labeled cells along the anterior–posterior axis was examined (Fig. 6N). The length of the labeled cell distribution area (a in Fig. 6N, inset) was divided by the diameter of the embryo (b in Fig. 6N, inset) and plotted on a graph (Shimada et al., 2008). At the 80% epiboly stage, the ratio was lower in the *β4GalT2* MO-in-

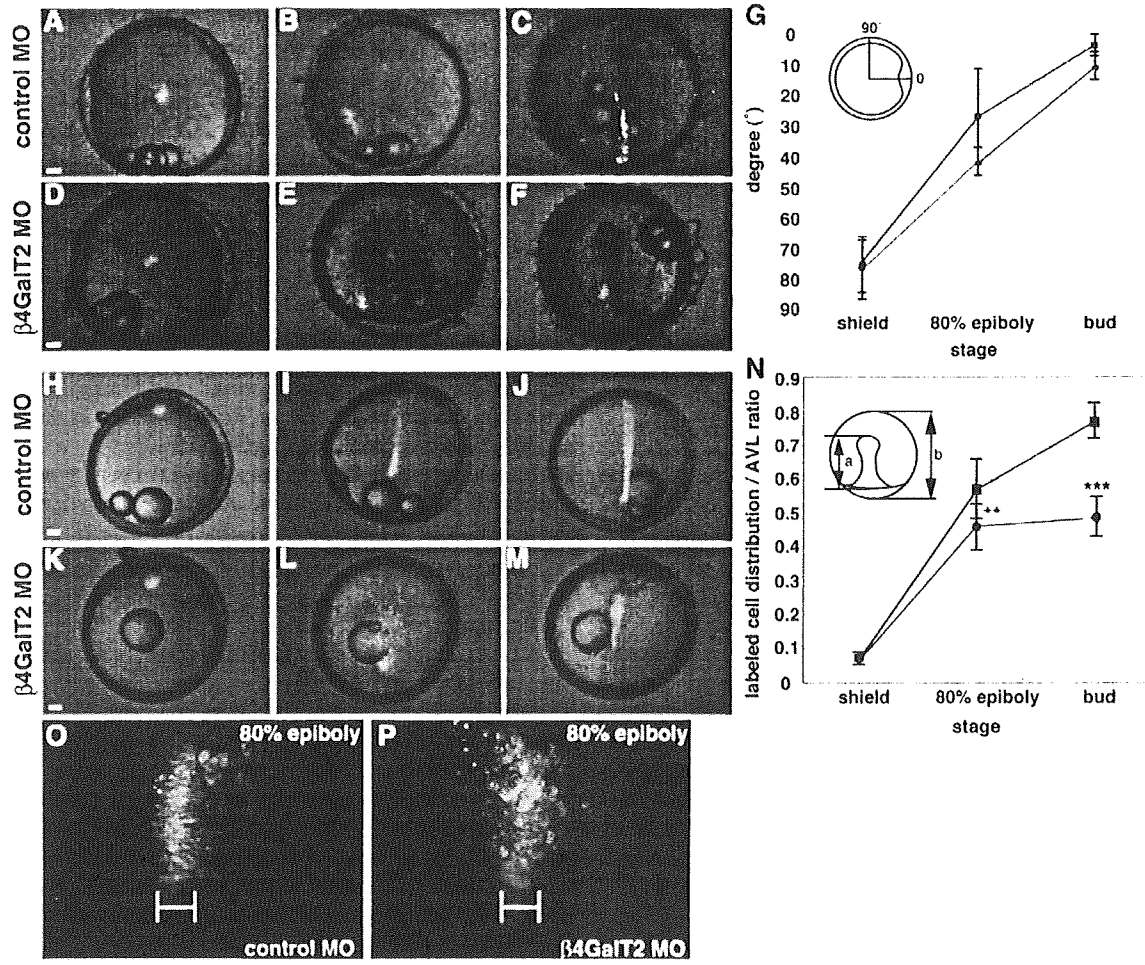

Fig. 6 – β4GalT2 activity is essential for proper extension movements during gastrulation. (A–F) Lateral mesendodermal cells were uncaged in control embryos (A–C) or in β4GalT2-depleted embryos (D–F). In the *β4GalT2* MO-injected embryos, the convergence of the lateral mesendodermal cells toward the dorsal side occurred normally. (G) A plot showing dorsal migration of the labeled cell groups in the control embryos ($n = 23$, blue) and the *β4GalT2* MO-injected embryos ($n = 21$, red). (H-M) Axial mesendodermal cells were uncaged in control embryos (H–J) or in β4GalT2-depleted embryos (K–M). At the 80% epiboly stage, anterior movement of the marked cells occurred in the *β4GalT2* MO-injected embryos (L), as well as in the control embryos (I); however, many labeled cells were not incorporated into the embryonic body. At the bud stage, labeled cells were observed in the embryonic body, but extension was severely perturbed in the *β4GalT2* MO-injected embryos (M). (N) A plot showing the length of the labeled cell distribution area (a)/animal–vegetal length (AVL; b) ratio, determined by morphometric analysis of the control ($n = 15$, blue) and *β4GalT2* MO-injected embryos ($n = 12$, red). (O, P) At the 80% epiboly stage, mediolateral cell intercalation was observed in the posterior tissue of the control embryos. In contrast, at the same stage, mediolateral cell intercalation was seemingly disturbed, and many labeled cells remained round in *β4GalT2* MO-injected embryos. The white symbol denotes the width of the embryonic body. Bar: 100 μm. (A,D) Lateral view, dorsal is to the right; (B, C, E, F, H–M) dorsal view, animal pole is to the top. $^{**}P < 0.01$, $^{***}P < 0.001$ compared with the control embryos according to the t-test.

jected embryos than in the control embryos, and at the bud stage, the difference in the ratio significantly increased (Fig. 6N; t-test, $P < 0.001$). Mediolateral cell intercalation was prominently observed in the control embryos at this stage, as the labeled midline cells became mediolaterally polarized, had an elongated shape, and cohered with each other (Fig. 6O). In contrast, the labeled cells remained round and failed to form a rigid cohesive structure in the *β4GalT2* MO-injected embryos (Fig. 6P). To directly assess the shape of the axial mesodermal cells in more detail, we injected RNA for cell membrane-targeted green fluorescent protein and observed the cells at high magnification with confocal microscopy (Fig. 7). In the control embryos, the cells at the dorsal midline became polarized and mediolaterally elongated at the 90% epiboly stage (Fig. 7A). On the other hand, the cells around the midline failed to elongate in the *β4GalT2* MO-injected embryos (Fig. 7B). At the segmentation stage, the notochord was clearly seen in the trunk region of the control embryos (Fig. 7C

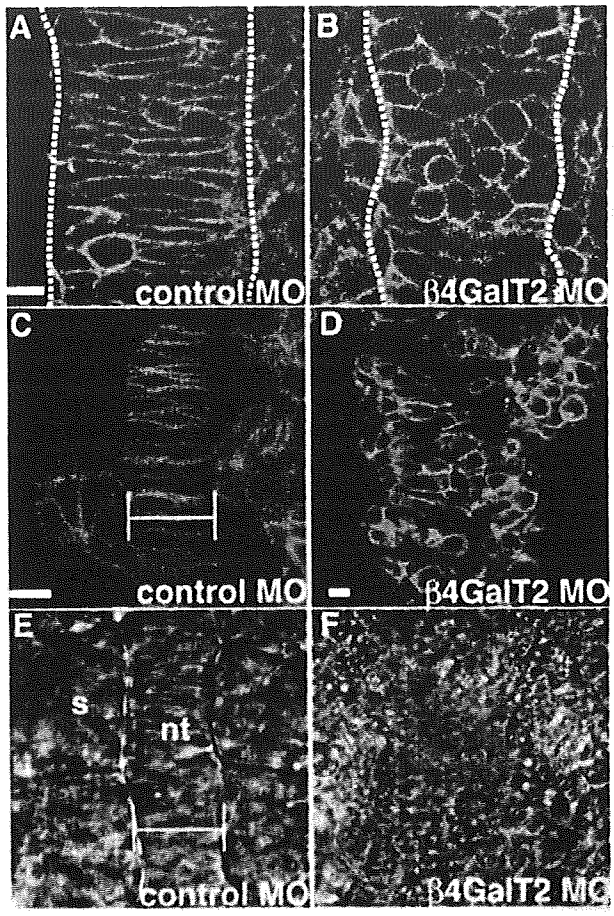

Fig. 7 – β4GalT2-depleted embryos show defective mediolateral cell intercalation. RNA encoding membrane-targeted green fluorescent protein was injected in conjunction with MO into two-cell stage embryos, and the morphology of the dorsal midline tissue was observed at the cellular level using confocal microscopy. (A,B) Dorsal view at the 90% epiboly stage, animal to the top. The dorsal midline tissue is located at the region between the two white dotted lines. (C–F), Dorsal view at the segmentation stage, anterior to the top. The panels E and F show Nomarski images of the areas shown in C and D, respectively. Note that the cells are laterally elongated and the form the notochord in control embryos, but the cells at identical locations failed to acquire the necessary polarity to form an organized midline structure in the *β4GalT2* MO-injected embryos. The white symbols in panels C and E denote the width of the notochord. nt, notochord; s, somite. Bars: 10 μm in all the panels.

and E). In sharp contrast, the cells at the dorsal midline failed to form an organized structure when β4GalT2 was depleted (Fig. 7D and F). These results suggest that mediolateral cell intercalation, which drives the extension movements at the dorsal midline, is disturbed in β4GalT2-depleted embryos. Taken together, we concluded that β4GalT2 is essential for mediolateral cell intercalation and thus normal extension movements.

2.6. *The cell-autonomous requirement of β4GalT2 in mediolateral cell intercalation*

The above observations indicated that β4GalT2 is required for mediolateral cell intercalation during late gastrulation. Various factors function in this process in either a cell-autonomous or non-cell-autonomous manner (Solnica-Krezel, 2005). In order to examine whether β4GalT2 is cell-autonomously required for this process, we carried out transplantation experiments, as outlined in Fig. 8A. As donor embryos, we injected either Rhodamine–dextran (red) with control MO or FITC-dextran (green) with *β4GalT2* MO into 1-cell stage embryos. At the shield stage, cells from the embryonic shield region of donors were aspirated, mixed, and transplanted into the corresponding region of host embryos at the same stage. As a control experiment, we injected fluorescent dyes without MO into donor embryos and transplanted the cells from these donor embryos into host embryos. At the segmentation stage,

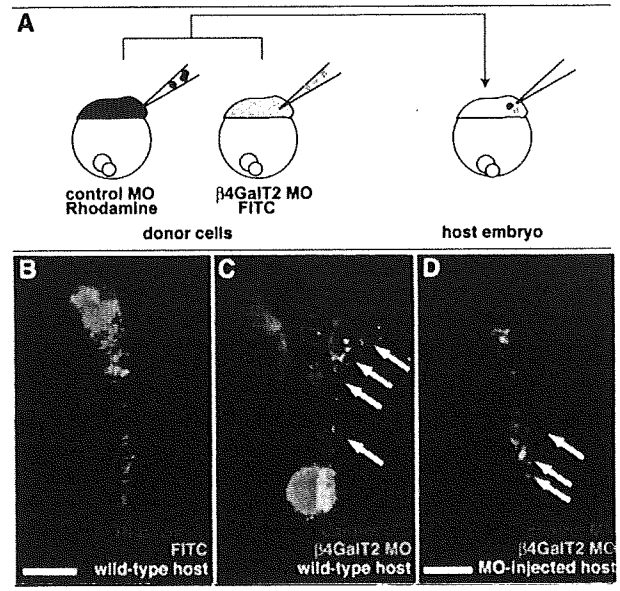

Fig. 8 – β4GalT2 functions cell-autonomously in cell intercalation during late gastrulation. (A) A schematic representation of the transplantation experiments. Donor cells from embryos injected with *β4GalT2* MO (green) or control MO (red) were transplanted simultaneously into the deep layer of the shield in wild-type hosts at the shield stage. (B) Donor cells in embryos injected with FITC-dextran or Rhodamine-dextran were transplanted into the deep layer of the shield in wild-type hosts. Both donor cells were incorporated into the embryonic body at 1 dpf. (C) Donor cells from embryos injected with *β4GalT2* MO (green) or control MO (red) were transplanted into wild-type hosts. The *β4GalT2* MO-injected cells (green) failed to polarize and become incorporated into the midline, although the control MO-injected cells (red) migrated into the axial midline tissue, which showed stripes called 'cellular strings'. (D) The donor cells were transplanted as in (C), except that *β4GalT2* MO-injected host embryos were used. (B–D) Dorsal view, animal pole is to the top. Bar: 100 μm.

cell populations from both donor embryos were incorporated into the embryonic body axis and consequently formed a band of mediolaterally elongated cells known as 'cellular strings' in the midline tissue ($n = 8/8$, Fig. 8B). In contrast, when MO-injected cells were transplanted into wild-type host embryos, the *β4GalT2* MO-injected green cells failed to be incorporated into the midline tissue including notochord and instead remained round (Fig. 8C, white arrows), whereas the control MO-injected red cells migrated into the midline tissue and showed an elongated shape ($n = 10/10$). As a complementary experiment, we next transplanted the donor cells into *β4GalT2* MO-injected host embryos. The control cells were incorporated into the midline tissue and seemed to form an organized axial structure to some extent. In contrast, some donor cells injected with *β4GalT2* MO were also incorporated into the midline tissue, but other cells were excluded from this structure ($n = 10/13$, Fig. 8D, arrows). These results suggest that β4GalT2 functions cell-autonomously, but not non-cell-autonomously, in the axial cells that take part in mediolateral cell intercalation during late gastrulation.

2.7. *Enhanced apoptosis in β4GalT2-depleted embryos cannot account for the defective extension movement*

While analyzing the phenotype of *β4GalT2* MO-injected embryos, we noticed that an area appeared as a dark shadow around the embryonic body (for example, see Fig. 6E). Closer examination revealed that this dark area contained apparently unhealthy cells that were detached from the embryonic body. Therefore, we carried out TUNEL staining of the embryos at various stages and found that a lot more apoptotic cells appeared in the *β4GalT2* MO-injected embryos than in the control from the 50% epiboly stage onward (Fig. S3). These results raise the possibility that enhanced apoptosis, not defective mediolateral cell intercalation, causes the phenotypic abnormalities observed in *β4GalT2* MO-injected embryos. To test this possibility, we used Bcl-xL, a well-known inhibitor of apoptosis (Boise et al., 1993). When *Bcl-xL* RNA was co-injected with *β4GalT2* MO, apoptosis was efficiently blocked (Fig. S4); however, the phenotypic abnormalities such as the cyclopia and impaired segmentation of somites were still observed, although the head hypoplasia was partially rescued (Fig. 9A and B and data not shown). Moreover, when the anterior–posterior length of the embryonic body was measured, it became obvious that the defective elongation caused by β4GalT2 depletion persisted even when apoptosis was blocked (Fig. 9C). Together, these results demonstrate that although apoptotic cell death was enhanced in the β4GalT2-depleted embryos, blockade of apoptosis did not rescue the phenotypic abnormalities. Therefore, we conclude that the enhanced apoptosis observed does not fully account for the defective extension movement observed in β4GalT2-depleted embryos.

3. Discussion

3.1. *β4GalT2 activity is cell-autonomously required for the extension movement mediated by mediolateral cell intercalation during medaka gastrulation*

Gastrulation is the most critical step in morphogenesis during vertebrate development. In fish, it consists of coordinated cell movements such as epiboly, internalization, convergence, extension, and mediolateral cell intercalation (Myers et al., 2002; Solnica-Krezel, 2005). Mediolateral cell intercalation is defined as a process arising at the dorsal

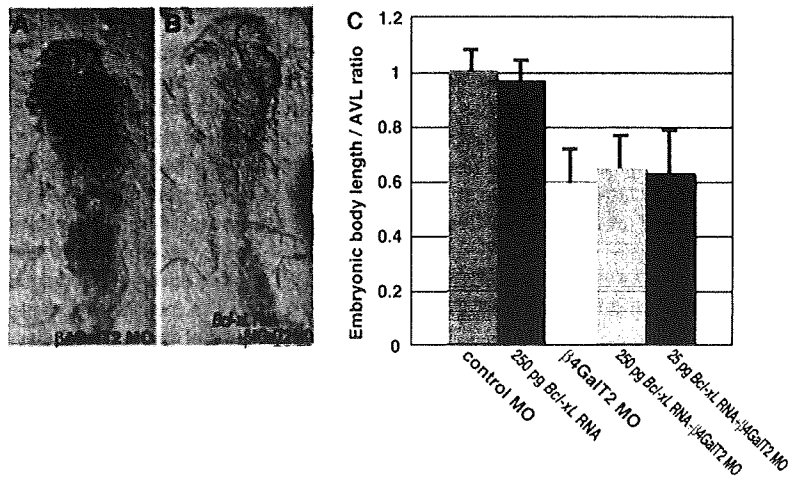

Fig. 9 – Enhanced apoptosis in β4GalT2-depleted embryos cannot account for the extension defects. (A,B) Co-injection of Bcl-xL RNA failed to rescue the phenotypic abnormalities caused by β4GalT2 depletion. Dorsal view at 1 dpf, anterior to the top. (C) Graph showing the embryonic body length/animal–vegetal length (AVL) ratio, as determined by morphometric analysis in control embryos ($n = 29$, blue), Bcl-xL RNA-injected embryos ($n = 27$, red), *β4GalT2* MO-injected embryos ($n = 30$, yellow), embryos co-injected with *β4GalT2* MO and 250 pg or 25 pg Bcl-xL RNA ($n = 31$ and 26, green and purple, respectively). *β4GalT2* MO-injected embryos exhibited defective elongation ($P < 0.001$compared with control in t-test). Co-injection of Bcl-xL RNA at either dose failed to rescue this defect ($P < 0.001$ compared with the control according to the t-test at both doses; no statistical significance between the *β4GalT2* MO-injected embryos and embryos co-injected with *β4GalT2* MO and Bcl-xL RNA).

midline, in which cells are morphologically transformed into a mediolaterally elongated shape, and these cells then intercalate with their neighboring cells. This in turn drives convergence and extension movements, resulting in narrowing of embryonic tissues mediolaterally and their anterior–posterior elongation, respectively (Keller et al., 2000). In this study, we demonstrated that β4GalT2 activity plays essential roles during gastrulation in cells undergoing mediolateral cell intercalation. The lines of evidence supporting our idea are as follows. First, the morphological defects observed in the β4GalT2-depleted embryos were rescued by co-injection of wild-type *β4GalT2* RNA, but not by mutant *β4GalT2* RNA encoding the enzyme without β-1,4-galactosyltransferase activity (Fig. 3), demonstrating that enzymatic activity is essential for this process. Second, β4GalT2-depleted medaka embryos showed a shortened body axis (Fig. 6), and direct assessment of cell shape in the midline tissue using confocal microscopy revealed that the axial cells of the β4GalT2-depleted embryos failed to mediolaterally elongate to form the notochord, which is indicative of impaired mediolateral cell intercalation. (Fig. 7). These observations indicate that the extension movement mediated by cell intercalation is defective in these embryos. Mesoderm induction and organizer formation appeared to occur normally in the β4GalT2-depleted embryos (Fig. 5), which is consistent with the observation that β4GalT2 is specifically required for cellular behavior during late gastrulation (Fig. 4). Finally, β4GalT2-depleted cells failed to contribute to the midline tissue when transplanted into wild-type host embryos (Fig. 8). This indicates that β4GalT2 is cell-autonomously required for mediolateral cell intercalation during the extension movement. Thus, we conclude that β4GalT2 activity is essential in cells undergoing mediolateral cell intercalation during medaka gastrulation. Considering that the size of the *β4GalT2* MO-injected embryos was much smaller than that of the control embryos (Figs. 3 and 4), together with the observation that there are cells which seem to be detached from the embryonic body (see Fig. 6E; dark shadows around the forming embryonic body represent apparently unhealthy cells), it is also possible that increased apoptosis and/or retardation of cell proliferation may occur in the absence of β4GalT2 to contribute to the observed phenotype. We therefore carried out TUNEL staining of the embryos and found that apoptotic cell death was indeed enhanced in the β4GalT2-depleted embryos. However, the enhanced apoptosis could not have been the main cause of the phenotypic defects of β4GalT2-depleted embryos, as these defects were still observed when apoptosis was efficiently blocked by co-injection of *Bcl-xL* RNA (Fig. 9).

3.2. *A comparison of β4GalT2-depleted embryos with zebrafish and medaka mutants showing similar phenotypes*

In this study, we used medaka as a model organism and found that the mediolateral cell intercalation and extension movements are impaired in β4GalT2-depleted embryos. The molecular mechanisms underlying gastrulation movements have been investigated by the use of various zebrafish mutants showing defective morphogenesis during this process. The basic mechanisms governing the gastrulation process seem to be widely well-conserved among vertebrates. In medaka and zebrafish, both teleost fish, these processes are quite similar (Solnica-Krezel, 2005; Trinkaus, 1998; Trinkaus et al., 1992). Therefore, we can discuss the possible cause of the phenotype found in the β4GalT2-depleted medaka embryos in the light of our knowledge of zebrafish mutants that show similar abnormalities in embryogenesis including during the process of convergence and extension movements.

The components of the Wnt/planar cell polarity (PCP) pathway are conceivable candidates to be affected in β4GalT2-depleted embryos, as the genetic mutation of the components of this pathway also causes abnormalities in mediolateral cell intercalation and convergence and extension movements. In this pathway, the binding of secreted glycoprotein ligands (Wnt5 or Wnt11) to their cognate receptor leads to cytoskeletal rearrangement mediated by small GTPases such as RhoA, Rac1 and, Cdc42. Cytoskeleton rearrangement regulated by the Wnt/PCP pathway is required for cells to acquire polarity and undergo morphological transformation into an elongated shape (Mlodzik, 1999; Winter et al., 2001). In the zebrafish mutants *wnt5/pipetail* (*ppt*) and *wnt11/silverblick* (*slb*), mediolateral cells fail to acquire the polarity required for proper mediolateral cell intercalation, resulting in shortening of the body axis and cyclopia (Heisenberg et al., 2000; Kilian et al., 2003; Lele et al., 2001). In addition, mutants of other components of the Wnt/PCP pathway downstream of *wnt5/11*, such as *dsh*, *prickle1*, and *rock2*, share similar abnormalities (Heisenberg et al., 2000; Marlow et al., 2002; Veeman et al., 2003). Importantly, mesoderm induction and organizer formation remain intact in these mutants. These phenotypes are very similar to that of β4GalT2-depleted embryos, in which mediolateral cell intercalation is disrupted. Therefore, it is possible that β4GalT2 also plays a regulatory role in the Wnt/PCP pathway, although it is currently unclear where and how this enzyme could be integrated into the pathway.

However, it should be noted that there are some differences between the Wnt/PCP pathway mutants and β4GalT2-depleted embryos. For example, the expression of paraxial mesoderm markers such as *myoD* and *papc* was not detected at the early segmentation stage in these embryos (data not shown). In addition, β4GalT2-depleted embryos showed relatively normal convergence of the lateral mesoderm while its extension was more severely defective (see Fig. 6). These results, coupled with the observation that the prechordal plate in β4GalT2-depleted embryos seems to be smaller than that in the control embryos (see Fig. 5), suggests impairment of the anterior migration of the mesendoderm in β4GalT2-depleted embryos besides extension movement defects.

The medaka maternal-zygotic mutant for *fibroblast growth factor receptor 1* (*fgfr1*) exhibits a phenotypic resemblance to β4GalT2-depleted embryos (Shimada et al., 2008). In this mutant, anterior migration of the axial mesoderm is disrupted, and the expression of axial and paraxial mesoderm markers is diminished at the segmentation stage, indicating that signaling through Fgfr1 is required for this process. For extension of the embryonic body, the coordinated execution of anterior migration and cell intercalation at the axial mesendoderm, including the prospective prechordal plate and notochord, is essential. The phenotypes observed in the trunk–tail region of the β4GalT2-depleted embryos and *fgfr1* mutants are

quite similar and are caused by defective extension movements in both cases, although there are marked differences in their overall phenotypes (Shimada et al., 2008). Interestingly, we found that the expression of sprouty4, a well-established target gene for Fgf signaling, was downregulated in the β4GalT2-depleted embryos at the 90% epiboly stage, when mediolateral cell intercalation is actively taking place (Fig. S2C). This suggests that Fgf signaling is somehow weakened in the absence of β4GalT2, although it is possible that the development of the tissues with sprouty4 expression was disturbed.

To test the possibilities described above, we co-injected *β4GalT2* MO and constitutively active (ca-) RhoA, ca-Rac1, or ca-cdc42 RNA, which functions downstream of the noncanonical Wnt signaling pathway (Choi and Han, 2002; Habas et al., 2003, 2001; Penzo-Mendez et al., 2003) or ca-H-Ras RNA, which acts downstream of the Fgf signaling pathway (Umbhauer et al., 2000). As a result, the co-injection of all tested RNA could not rescue the abnormal phenotype observed in the β4GalT2-depleted embryos (data not shown).

As mentioned above, β4GalT2-depleted embryos seem to exhibit complex abnormalities resulting from defects in several elementary steps such as cell motility, cell–cell interactions, and apoptosis during embryogenesis, because depletion of β4GalT2 alters the glycosylation of many glycoproteins. Basically, the loss-of-function approach of glycosyltransferases makes it more difficult to address the roles of glycans, especially in signaling pathways during vertebrate development. In spite of this, our data highlighted that β4GalT2 is mainly involved in regulating mediolateral cell intercalation and extension movement during medaka gastrulation. Furthermore, our findings also raise the possibility of a connection between β4GalT2 activity and the Wnt/PCP and Fgf signaling pathways. We believe that understanding the function of glycans in particular signaling pathways will bring new insights into the study of developmental biology; however, their roles in signaling pathways during vertebrate development are largely unknown.

3.3. *How does β4GalT2 regulate mediolateral cell intercalation at the molecular level?*

Members of the β4GalT family catalyze the transfer of Gal from UDP-Gal to GlcNAc on nascent glycoconjugates, although each member of the family has a different acceptor substrate specificity (Hennet, 2002). The substrate specificity of mammalian β4GalT2 has been studied in detail and it has been shown to be involved in the biosynthesis of N-glycans on proteins (Almeida et al., 1997; Sato et al., 1998). In this study, we demonstrated that the galactosyltransferase activity of β4GalT2 is indispensable for mediolateral cell intercalation and thus extension movement, suggesting that the N-glycans biosynthesized by β4GalT2 have important roles in these processes. In zebrafish, there are several reports in which a link between glycans and convergence and extension is suggested. For example, the mutant of *knypek/glypican4*, which encodes a member of the membrane-bound type of heparansulfate proteoglycans, exhibits features of convergence and extension disorder, such as a shortened body axis and broadened axial tissue (Topczewski et al., 2001). Embryos injected with MO for *hyaluronan synthase 2* (*has2*) also display deficiencies in directed cell migration during gastrulation, though axial tissue extension occurs normally. Has2 is an enzyme that is necessary for biosynthesis of the glycosaminoglycan hyaluronan, a high molecular weight extracellular polysaccharide (Bakkers et al., 2004). However, it seems unlikely that β4GalT2 is involved in the biosynthesis of glycans affected in these mutants and morphants, since β4GalT2 has specificity towards N-glycans as mentioned above. Therefore, disruption of glycosylation in these glycoproteins, which are already known to regulate convergence and extension, would not account for the defects observed in β4GalT2-depleted embryos. As mentioned above, the Fgf signaling pathway could be modified in a glycan-dependent manner, as Fgfr1 is an N-glycosylated protein, and the glycans are known to determine its signaling efficiency by altering its interaction with its ligand and the heparansulfate co-receptor (Duchesne et al., 2006). It is also possible that the Wnt/PCP pathway is modified, as N-glycans are essential for the secretion of Wnt-3a and -5a from cultured cells (Komekado et al., 2007; Kurayoshi et al., 2007). Based on the mutant phenotype and its glycosylation properties, cell adhesion molecules, such as cadherins and protocadherins, could also be affected in *β4GalT2* MO-injected embryos. It was reported that E-cadherin is expressed in dorsal tissue at the gastrulation stage (Shimizu et al., 2005), and its ability to form homodimers depends on N-glycosylation (Liwosz et al., 2006; Zhao et al., 2007). It would be interesting to examine if the glycans on E-cadherin are altered in *β4GalT2* MO-injected embryos.

Recently, it was reported that zebrafish embryos in which β4GalT1 expression had been depleted by MO injection also exhibit defective convergence and extension (Machingo et al., 2006). The zebrafish β4GalT1 shows the highest sequence similarity to β4GalT1 among the human β4GalT family, whereas medaka β4GalT2 shows the highest sequence similarity to human β4GalT2. Additionally, in zebrafish, there is a gene, which has a higher similarity to medaka β4GalT2 than to zebrafish β4GalT1 (Machingo et al., 2006). The nucleotide sequence of the gene (zebrafish β4GalT2; Genbank Accession No. NM_001128385) considerably differs from that of zebrafish β4GalT1. A phylogenetic analysis among the three genes (medaka β4GalT2, zebrafish βGalT1 and β4GalT2) also demonstrated that medaka β4GalT2 is closer to zebrafish β4GalT2 than to zebrafish β4GalT1. Therefore, the cloned β4GalT, medaka β4GalT2 is not the ortholog of zebrafish β4GalT1 but rather that of zebrafish β4GalT2. Among the human β4GalT family, however, β4GalT1 and β4GalT2 are the closest subtypes in terms of both amino acid sequence and substrate specificity. Moreover, medaka β4GalT2 and zebrafish β4GalT1 display almost identical expression patterns, and the phenotypic features observed in respective MO-injected embryos are similar. Therefore, these two distinct β4GalT may partially share substrates involved in early development and function coordinately in this process. In fact, we found that medaka β4GalT1 is expressed at both the blastula and gastrula stages (data not shown). We thus performed a rescue experiment in which mouse β4GalT1 RNA was co-injected with *β4GalT2* MO. This resulted in the suppression of loss of the β4GalT2 phenotype, suggesting that mouse β4GalT1 is able to compensate for the loss of β4GalT2 when

overexpressed (Fig. S5). Despite the close substrate specificity shared by β4GalT1 and β4GalT2 in mammals, it is also reported that there are some differences. For example, in humans, the galactosyltransferase activity of β4GalT2 against O-fucosylated glycans is higher than that of β4GalT1 (Sasaki et al., 2005). In the future, identification of the substrates of β4GalT2 is essential, as it would provide a more detailed understanding of the role of glycans during gastrulation.

In conclusion, we have demonstrated that β4GalT2 is required for proper mediolateral cell intercalation and thus extension movement during medaka gastrulation. β-1,4-Galactosyltransferase activity is cell-autonomously required in this context, suggesting that the glycans synthesized by this enzyme are essential for these processes. Identification of the target molecules that carry these glycans will lead to better understanding of the novel roles of β-1,4-galactosylated glycans during early vertebrate development.

4. Materials and methods

4.1. *Medaka maintenance, embryo production and staging*

Medaka of the d-rR strain were maintained under an artificial photoperiod of 14L:10D, at an ambient temperature of 27°C. Embryos were produced by natural mating and staged according to morphology as described (Iwamatsu, 2004).

4.2. *Molecular cloning of medaka β4GalT2 cDNA and phylogenetic analysis among human β4GalT family*

The NBRP medakafish genome project (http://www.shigen.nig.ac.jp/medaka/genome/top.jsp) entry for β4GalT2 appeared to correspond to the 5′- and 3′-ends of human β4GalT2. Based on these sequences, primers (forward: 5′-CTTGAATTCATGACCCGGCTGATGTTGGG-3′, reverse: 5′-GTGAATTCCTAACCTGTGATGGGCCGGGG-3′, newly created EcoRI sites are underlined) were designed and used for cDNA cloning by RT-PCR. Total RNA was prepared from pooled medaka embryos (0–8 days post-fertilization) by TRIzol (Invitrogen, Carlsbad, CA), and then cDNA was synthesized by Superscript II reverse transcriptase (Invitrogen). The 1.1 kbp PCR product was cloned into the pGEM-T Easy vector (Promega, Madison, WI), and then the nucleotide sequence was analyzed. To clone 5′-UTR, RT-PCR was performed using a SMART-RACE cDNA amplification kit (BD Biosciences, Franklin Lakes, NJ) according to the manufacturer's protocol. Phylogenetic analysis among vertebrate β4GalT, as described below, was performed by the multiple sequence alignment program ClustalW. hsβ4GalT1 (*Homo sapiens*, X14085); hsβ4GalT2 (AB024434); hsβ4GalT3 (AB024435); hsβ4GalT4 (AB024436); hsβ4GalT5 (AB004550); hsβ4GalT6 (AB024742); hsβ4GalT7 (AJ005382); trβ4GalT2 (*Takifugu rubripes*, Ensembl Accession No. SINFRUT00000144236); mmβ4GalT2 (*Mus musculus*, Genbank Accession No. AB019541).

4.3. *Quantitative RT-PCR*

Fifty embryos from each stage were harvested and lysed in TRIzol for total RNA extraction. Total RNA was digested with DNaseI before the PCR to prevent genomic DNA contamination. One microgram of total RNA was used per 25 μl reaction. The PCR was performed with a Chromo 4 Real-Time System (Bio-Rad, Hercules, CA) using SYBR green I. The primers used were as follows:

β-actin forward: 5′-ACCCACACAGTGCCCATCTACGA-3′,
β-actin reverse: 5′-AGACAGCACAGTGTTGGCGTACAG-3′,
β4GalT2 forward: 5′-ATGACCCGGCTGATGTTGGGACGGA-3′,
β4GalT2 reverse: 5′-AAGACCAGGCGGGTTCTCAGGACA-3′.

Each sample was run in triplicate and then averaged. Quantification of relative expression was carried out using *β-actin* expression as a standard.

4.4. *RNA and morpholino oligonucleotides injection and TUNEL staining*

Capped RNA was synthesized using a RiboMax large scale RNA production kit (Promega). After the reaction, synthesized RNA was purified using the RNeasy Mini Kit (Qiagen, Hilden, Germany) and diluted with RNase-free water to a final concentration of 400 ng/μl (medaka *β4GalT2* and *mut β4GalT2*). RNA (200 pg) was injected into the cells of one- to two-cell-stage embryos. For the *Bcl-xL*, mouse *β4GalT1*, constitutively active (ca-) RhoA, ca-Rac1, ca-Ras, and ca-Cdc42 RNA coinjection experiments, RNA were synthesized, respectively, as above and injected at the dose described. Morpholino antisense nucleotides (MOs) were designed to bind to sequences flanking and including the initiating methionine codon and obtained from Gene Tools, LLC (Philomath, OR). The sequences of the MO were as follows (the sequence complementary to the predicted start codon is underlined): *β4GalT2* MO: 5′-CGTCCCAACATCAGCCGGGTCATGG-3′, *β4GalT2* MO2: 5′-CCGATGGAGGTTACCGTCCTGCGAC-3′, control MO: 5′-CGTCCgAAgATCAaCCGGGTgATcG-3′. MO were dissolved and diluted in Yamamoto's Ringer solution (Yamamoto, 1954), and 4 ng were injected into the cells of one- to two-cell-stage embryos. TUNEL staining was carried out using the DeadEnd Fluorometric TUNEL system (Promega) according to the manufacturer's instructions.

4.5. *Site-directed mutagenesis of β4GalT2*

Trp288 (indicated by asterisks in Fig. 1A) in β4GalT2 was substituted for Ala according to the procedure described previously (Ramasamy et al., 2003). The following primers were used for site-directed mutagenesis: 5′-GAGTACTGGG CGCGGGGGGGGAGGAC-3′ and 5′-GTCCTCCCCCCCGGCGCCC AGTACTC-3′ (the Ala codon introduced is underlined).

4.6. *Whole-mount in situ hybridization*

Whole-mount *in situ* hybridization was performed as described (Loosli et al., 1998). Briefly, staged embryos were fixed in 4% paraformaldehyde and dehydrated in methanol. Following rehydration in phosphate-buffered saline/0.1% Tween 20, the embryos were prehybridized for 2 h at 65°C. Hybridization with gene-specific probes was conducted overnight at 65°C. DIG-labeled probes were detected with anti-DIG antibody (Roche, Basel, Switzerland) and visualized with BM purple (Roche). The following antisense digoxigenin-

labeled probes were used: *no tail* (Araki et al., 2001), *bmp2* (medaka EST Database, Accession No. MF01SSA199F01), *spadetail* (MF01SSA103E01), *goosecoid* (MF015DA014K11), *six3* (MF015DA 006K02), *pax2* (MF01SSA182E11), *chordin* (Ensembl Accession No. ENSORLT00000011913, nucleotide sequence 1577–2135), *sox17α* (MF01SSA074A09), *papc* (ENSORLT00000022242), and *β4GalT2* (nucleotide sequence 39–542). The probes were synthesized using a DIG RNA labeling Kit T7/SP6 (Roche) or T3 polymerase (Applied Biosystems, Foster City, CA) and were purified using the RNeasy Mini Kit.

4.7. *Cell tracing experiment and confocal microscopic analysis*

One-cell stage embryos were injected with 0.5 nl of 1.5% 4,5-dimethoxy-2-nitrobenzyl (DMNB)-caged fluorescein-dextran (M_r 3000, Molecular Probes, Eugene, OR) and 4 ng of the *β4GalT2* MO or control MO. The embryos were then grown in the dark until the shield stage. To uncage the dye, a beam of ultraviolet light ($\lambda = 364$ nm) generated using a FITC filter set was directed for 5 s at the dorsal or lateral blastoderm margin (Kozlowski et al., 1997; Sepich et al., 2000). The location of the cells containing the uncaged fluorescein-dextran was monitored by observation using a stereomicroscope Leica MZ16FA fitted with a Leica DFC 500 camera (Leica Microsystems, Wetzlar, Germany) and recorded at the indicated stages. For confocal microscopic analyses, the embryos were observed using the Fluoview system (OLYMPUS, Tokyo, Japan).

4.8. *Transplantation experiment*

The transplantation experiment was performed as described (Shimada et al., 2008). Donor embryos were injected at the 1-cell stage either with 0.5 nl of 4% rhodamine-dextran (M_r 10,000, Molecular Probes) and 4 ng of control MO or with 0.5 nl of 4% fluorescein isothiocyanate (FITC)-dextran (M_r 10,000, Molecular Probes) and 4 ng of *β4GalT2* MO. The donor embryos were grown until the shield stage. A small population of deep cells from each donor embryo (i.e. injected with rhodamine and control MO or FITC and *β4GalT2* MO) was aspirated using a micropipette, followed by transplantation into either wild-type or *β4GalT2* MO-injected host embryos at the embryonic shield. The locations of the labeled donor cells were monitored as described above.

4.9. *β-1,4-Galactosyltransferase activity assay*

β-1,4-Galactosyltransferase activity was measured as described previously (Oka et al., 1992; Sasaki et al., 2005) with modifications. As an acceptor substrate, asialo-agalacto-orosomucoid (AGOR) was prepared using asialo-orosomucoid (ASOR). ASOR (400 μg) was incubated with 20 mU *Streptococcus β-galacatosidase (Seikagaku corporation, Tokyo, Japan) in 200 μl of 100 mM acetate buffer pH 5.5 containing 10 mM $MnCl_2$ for 20 min at 37°C. Removal of the galactose residue was confirmed by reactivity loss with RCA120 lectin (data not shown), which recognizes the terminal galactose residues. The reaction mixture was incubated for 30 min at 60°C to denature the β-galactosidase and then neutralized by the addition of 30 μl of 1 M Tris–HCl, pH 8.5. To prepare the enzyme sources, control MO- and β4GalT2* MO-injected embryos were collected at the bud stage and dechorionated. The yolk was removed by pipetting in a balanced salt solution for medaka (Iwamatsu and Onitake, 1983), and the embryos were transferred into extraction buffer (20 mM Tris–HCl, pH 7.4, 150 mM NaCl, 1 mM EDTA, 1% Triton X-100, 0.5% deoxycholate and protease inhibitors). The proteins were extracted from the embryonic tissue in the buffer. After centrifugation at 15,000*g* for 10 min, the resultant supernatant was used as an enzyme source. An equivalent amount of each enzyme solution was incubated at 37°C for 2 h in a 50-μl reaction mixture comprising 20 μl of the acceptor substrate, AGOR as described above, 100 μM UDP-[^{14}C]-galactose (200,000 dpm). After incubation, the assay mixture was spotted onto a 2.5-cm Whatman No.1 disc. The disc was washed with a 10% trichloroacetic acid solution three times, followed by with ethanol/ether (2:1, v/v) and then with ether. The disc was dried, and the radioactivity was counted with a liquid scintillation counter.

Acknowledgements

We thank Drs. Masahiko Hibi (RIKEN), Hiroki Kuroda (Shizuoka Univ.), Atsuko Shimada (Tokyo Univ.), Hiromu Takematsu (Kyoto Univ.), and the members of our laboratories for their critical discussion and comments on the manuscript. We acknowledge Mizue Hanaki and Miwako Tonoyama for their excellent fish care. The GAP43-Venus vector was a gift from Dr. Atsushi Miyawaki (RIKEN). The ca-H-Ras, ca-RhoA, ca-Rac1, and ca-Cdc42 vectors were provided by Dr. Manabu Negishi (Kyoto Univ.). The DNA clones containing *shh* and *ntl* cDNAs were a generous gift from Dr. Kazuo Araki (National Research Institute of Aquaculture). The *bmp2*, *axl*, *gsc*, sox17α, and *spt* cDNA were provided by The National Institute for Basic Biology and The University of Tokyo through the National Bio-Resource Project (NBRP) of the MEXT, Japan. This work was supported by a Grant-in-Aid for Creative Scientific Research (16GS0313 to S.O.) from the Ministry of Education, Culture, Sports and, Technology.

Appendix A. Supplementary data

Supplementary data associated with this article can be found, in the online version, at doi:10.1016/j.mod.2009.03.004.

REFERENCES

Almeida, R., Amado, M., David, L., Levery, S.B., Holmes, E.H., Merkx, G., van Kessel, A.G., Rygaard, E., Hassan, H., Bennett, E., Clausen, H., 1997. A family of human beta4-galactosyltransferases. Cloning and expression of two novel UDP-galactose:beta-n-acetylglucosamine beta1, 4-galactosyltransferases, beta4Gal-T2 and beta4Gal-T3. J. Biol. Chem. 272, 31979–31991.

Araki, K., Okamoto, H., Graveson, A.C., Nakayama, I., Nagoya, H., 2001. Analysis of haploid development based on expression patterns of developmental genes in the medaka *Oryzias latipes*. Dev. Growth Differ. 43, 591–599.

Bakkers, J., Kramer, C., Pothof, J., Quaedvlieg, N.E., Spaink, H.P., Hammerschmidt, M., 2004. Has2 is required upstream of Rac1

to govern dorsal migration of lateral cells during zebrafish gastrulation. Development 131, 525–537.
Boise, L.H., Gonzalez-Garcia, M., Postema, C.E., Ding, L., Lindsten, T., Turka, L.A., Mao, X., Nunez, G., Thompson, C.B., 1993. Bcl-x, a bcl-2-related gene that functions as a dominant regulator of apoptotic cell death. Cell 74, 597–608.
Campbell, R.M., Metzler, M., Granovsky, M., Dennis, J.W., Marth, J.D., 1995. Complex asparagine-linked oligosaccharides in Mgat1-null embryos. Glycobiology 5, 535–543.
Choi, S.C., Han, J.K., 2002. Xenopus Cdc42 regulates convergent extension movements during gastrulation through Wnt/Ca^{2+} signaling pathway. Dev. Biol. 244, 342–357.
Duchesne, L., Tissot, B., Rudd, T.R., Dell, A., Fernig, D.G., 2006. N-glycosylation of fibroblast growth factor receptor 1 regulates ligand and heparan sulfate co-receptor binding. J. Biol. Chem. 281, 27178–27189.
Grunewald, S., Matthijs, G., Jaeken, J., 2002. Congenital disorders of glycosylation: a review. Pediatr. Res. 52, 618–624.
Habas, R., Dawid, I.B., He, X., 2003. Coactivation of Rac and Rho by Wnt/Frizzled signaling is required for vertebrate gastrulation. Genes Dev. 17, 295–309.
Habas, R., Kato, Y., He, X., 2001. Wnt/Frizzled activation of Rho regulates vertebrate gastrulation and requires a novel Formin homology protein Daam1. Cell 107, 843–854.
Heisenberg, C.P., Tada, M., Rauch, G.J., Saude, L., Concha, M.L., Geisler, R., Stemple, D.L., Smith, J.C., Wilson, S.W., 2000. Silberblick/Wnt11 mediates convergent extension movements during zebrafish gastrulation. Nature 405, 76–81.
Hennet, T., 2002. The galactosyltransferase family. Cell. Mol. Life Sci. 59, 1081–1095.
Iwamatsu, T., 2004. Stages of normal development in the medaka *Oryzias latipes*. Mech. Dev. 121, 605–618.
Iwamatsu, T., Onitake, K., 1983. On the effects of cyanoketone on gonadotrophin- and steroid-induced in vitro maturation of Oryzias oocytes. Gen. Comp. Endocrinol. 52, 418–425.
Keller, R., Davidson, L., Edlund, A., Elul, T., Ezin, M., Shook, D., Skoglund, P., 2000. Mechanisms of convergence and extension by cell intercalation. Philos. Trans. R. Soc. Lond. B Biol. Sci. 355, 897–922.
Kido, M., Asano, M., Iwakura, Y., Ichinose, M., Miki, K., Furukawa, K., 1998. Presence of polysialic acid and HNK-1 carbohydrate on brain glycoproteins from beta-1,4-galactosyltransferase-knockout mice. Biochem. Biophys. Res. Commun. 245, 860–864.
Kilian, B., Mansukoski, H., Barbosa, F.C., Ulrich, F., Tada, M., Heisenberg, C.P., 2003. The role of Ppt/Wnt5 in regulating cell shape and movement during zebrafish gastrulation. Mech. Dev. 120, 467–476.
Kim, S.H., Yamamoto, A., Bouwmeester, T., Agius, E., Robertis, E.M., 1998. The role of paraxial protocadherin in selective adhesion and cell movements of the mesoderm during Xenopus gastrulation. Development 125, 4681–4690.
Komekado, H., Yamamoto, H., Chiba, T., Kikuchi, A., 2007. Glycosylation and palmitoylation of Wnt-3a are coupled to produce an active form of Wnt-3a. Genes Cells 12, 521–534.
Kozlowski, D.J., Murakami, T., Ho, R.K., Weinberg, E.S., 1997. Regional cell movement and tissue patterning in the zebrafish embryo revealed by fate mapping with caged fluorescein. Biochem. Cell. Biol. 75, 551–562.
Kurayoshi, M., Yamamoto, H., Izumi, S., Kikuchi, A., 2007. Post-translational palmitoylation and glycosylation of Wnt-5a are necessary for its signalling. Biochem. J. 402, 515–523.
Lele, Z., Bakkers, J., Hammerschmidt, M., 2001. Morpholino phenocopies of the swirl, snailhouse, somitabun, minifin, silberblick, and pipetail mutations. Genesis 30, 190–194.
Liwosz, A., Lei, T., Kukuruzinska, M.A., 2006. N-glycosylation affects the molecular organization and stability of E-cadherin junctions. J. Biol. Chem. 281, 23138–23149.
Lo, N.W., Shaper, J.H., Pevsner, J., Shaper, N.L., 1998. The expanding beta 4-galactosyltransferase gene family: messages from the databanks. Glycobiology 8, 517–526.
Loosli, F., Koster, R.W., Carl, M., Krone, A., Wittbrodt, J., 1998. Six3, a medaka homologue of the Drosophila homeobox gene sine oculis is expressed in the anterior embryonic shield and the developing eye. Mech. Dev. 74, 159–164.
Lowe, J.B., Marth, J.D., 2003. A genetic approach to Mammalian glycan function. Annu. Rev. Biochem. 72, 643–691.
Lu, Q., Hasty, P., Shur, B.D., 1997. Targeted mutation in beta1,4-galactosyltransferase leads to pituitary insufficiency and neonatal lethality. Dev. Biol. 181, 257–267.
Machingo, Q.J., Fritz, A., Shur, B.D., 2006. A beta1,4-galactosyltransferase is required for convergent extension movements in zebrafish. Dev. Biol. 297, 471–482.
Marek, K.W., Vijay, I.K., Marth, J.D., 1999. A recessive deletion in the GlcNAc-1-phosphotransferase gene results in peri-implantation embryonic lethality. Glycobiology 9, 1263–1271.
Marlow, F., Topczewski, J., Sepich, D., Solnica-Krezel, L., 2002. Zebrafish Rho kinase 2 acts downstream of Wnt11 to mediate cell polarity and effective convergence and extension movements. Curr. Biol. 12, 876–884.
McFarland, K.N., Warga, R.M., Kane, D.A., 2005. Genetic locus half baked is necessary for morphogenesis of the ectoderm. Dev. Dyn. 233, 390–406.
Mlodzik, M., 1999. Planar polarity in the Drosophila eye: a multifaceted view of signaling specificity and cross-talk. EMBO J. 18, 6873–6879.
Myers, D.C., Sepich, D.S., Solnica-Krezel, L., 2002. Convergence and extension in vertebrate gastrulae: cell movements according to or in search of identity? Trends Genet. 18, 447–455.
Oka, S., Terayama, K., Kawashima, C., Kawasaki, T., 1992. A novel glucuronyltransferase in nervous system presumably associated with the biosynthesis of HNK-1 carbohydrate epitope on glycoproteins. J. Biol. Chem. 267, 22711–22714.
Penzo-Mendez, A., Umbhauer, M., Djiane, A., Boucaut, J.C., Riou, J.F., 2003. Activation of Gbetagamma signaling downstream of Wnt-11/Xfz7 regulates Cdc42 activity during Xenopus gastrulation. Dev. Biol. 257, 302–314.
Ramasamy, V., Ramakrishnan, B., Boeggeman, E., Qasba, P.K., 2003. The role of tryptophan 314 in the conformational changes of beta1,4-galactosyltransferase-I. J. Mol. Biol. 331, 1065–1076.
Sasaki, N., Manya, H., Okubo, R., Kobayashi, K., Ishida, H., Toda, T., Endo, T., Nishihara, S., 2005. Beta4GalT-II is a key regulator of glycosylation of the proteins involved in neuronal development. Biochem. Biophys. Res. Commun. 333, 131–137.
Sato, T., Furukawa, K., Bakker, H., Van den Eijnden, D.H., Van Die, I., 1998. Molecular cloning of a human cDNA encoding beta-1,4-galactosyltransferase with 37% identity to mammalian UDP-Gal:GlcNAc beta-1,4-galactosyltransferase. Proc. Natl. Acad. Sci. USA 95, 472–477.
Sepich, D.S., Myers, D.C., Short, R., Topczewski, J., Marlow, F., Solnica-Krezel, L., 2000. Role of the zebrafish trilobite locus in gastrulation movements of convergence and extension. Genesis 27, 159–173.
Shimada, A., Yabusaki, M., Niwa, H., Yokoi, H., Hatta, K., Kobayashi, D., Takeda, H., 2008. Maternal-zygotic medaka mutants for fgfr1 reveal its essential role in the migration of the axial mesoderm but not the lateral mesoderm. Development 135, 281–290.
Shimizu, T., Yabe, T., Muraoka, O., Yonemura, S., Aramaki, S., Hatta, K., Bae, Y.K., Nojima, H., Hibi, M., 2005. E-cadherin is required for gastrulation cell movements in zebrafish. Mech. Dev. 122, 747–763.
Solnica-Krezel, L., 2005. Conserved patterns of cell movements during vertebrate gastrulation. Curr. Biol. 15, R213–R228.